Solid Earth, 11, 2169–2195, 2020
https://doi.org/10.5194/se-11-2169-2020

Solid Earth Open Access EGU

Structural control on fluid flow and shallow diagenesis: insights from calcite cementation along deformation bands in porous sandstones

Leonardo Del Sole[1], Marco Antonellini[1], Roger Soliva[2], Gregory Ballas[2], Fabrizio Balsamo[3], and Giulio Viola[1]

[1]BiGeA – Department of Biological, Geological and Environmental Sciences, University of Bologna, Via Zamboni 67, 40126 Bologna, Italy
[2]Laboratoire Géosciences Montpellier, Université de Montpellier, CNRS, Université des Antilles, Montpellier, France
[3]Next, Natural and Experimental Tectonic Research Group, Department of Chemistry, Life Sciences and Environmental Sustainability, University of Parma, Parco Area delle Scienze 157A, 43124 Parma, Italy

Correspondence: Leonardo Del Sole (leonardo.delsole@unibo.it)

Received: 9 May 2020 – Discussion started: 5 June 2020
Revised: 30 September 2020 – Accepted: 5 October 2020 – Published: 19 November 2020

Abstract. Porous sandstones are important reservoirs for geofluids. Interaction therein between deformation and cementation during diagenesis is critical since both processes can strongly reduce rock porosity and permeability, deteriorating reservoir quality. Deformation bands and fault-related diagenetic bodies, here called "structural and diagenetic heterogeneities", affect fluid flow at a range of scales and potentially lead to reservoir compartmentalization, influencing flow buffering and sealing during the production of geofluids. We present two field-based studies from Loiano (northern Apennines, Italy) and Bollène (Provence, France) that elucidate the structural control exerted by deformation bands on fluid flow and diagenesis recorded by calcite nodules associated with the bands. We relied on careful in situ observations through geo-photography, string mapping, and unmanned aerial vehicle (UAV) photography integrated with optical, scanning electron and cathodoluminescence microscopy, and stable isotope (δ^{13}C and δ^{18}O) analysis of nodules cement. In both case studies, one or more sets of deformation bands precede and control selective cement precipitation. Cement texture, cathodoluminescence patterns, and their isotopic composition suggest precipitation from meteoric fluids. In Loiano, deformation bands acted as low-permeability baffles to fluid flow and promoted selective cement precipitation. In Bollène, clusters of deformation bands restricted fluid flow and focused diagenesis to parallel-to-band compartments. Our work shows that deformation bands control flow patterns within a porous sandstone reservoir and this, in turn, affects how diagenetic heterogeneities are distributed within the porous rocks. This information is invaluable to assess the uncertainties in reservoir petrophysical properties, especially where structural and diagenetic heterogeneities are below seismic resolution.

1 Introduction

Porous rocks, such as sandstone and carbonate, are important reservoirs for geofluids. Structural and diagenetic processes commonly affect the petrophysical properties and reservoir quality in these rocks. The importance of the interaction between deformation and structures, fluid flow, and diagenetic processes has been emphasized only during the last 2 decades (e.g., see the recently coined term *structural diagenesis*; Laubach et al., 2010; Mozley and Goodwin, 1995; Eichhubl et al., 2009; Balsamo et al., 2012; Philit et al., 2015; Antonellini et al., 2017, 2020; Del Sole et al., 2020). If deformation influences diagenesis and vice versa, a feedback can eventually develop between these two processes. Early diagenesis influences the mechanical properties of rocks (Antonellini et al., 2020) and, in turn, their mechanical stratigraphy (Laubach et al., 2009; La Bruna et al., 2020). "Structural and diagenetic heterogeneities" (referred to as SDHs from now on) can determine the textural characteristics (e.g., grain

size, grain shape, relative proportion of grains, and matrix material) as well as the petrophysical and mechanical properties of the rock volume hosting them (Antonellini and Aydin, 1994; Aydin, 2000; Faulkner et al., 2010; Bense et al., 2013; Pei et al., 2015; Del Sole et al., 2020). Cement precipitation in granular porous siliciclastic rocks leads to porosity loss, reduction in permeability (Tenthorey et al., 1998; Morad et al., 2010), and, in turn, overall reservoir quality deterioration (Ehrenberg, 1990; Morad et al., 2010). Carbonate cement is commonly concentrated within a few specific horizons or nodules with various shapes and arrangements (Kantorowicz et al., 1987; Bjørkum and Walderhaug, 1990; Mozley and Davis, 1996), making porosity and permeability prediction more challenging (Davis et al., 2006; Morad et al., 2010). Furthermore, cement increases the mechanical strength of the host rock (Dvorkin et al., 1991; Bernabé et al., 1992; Boutt et al., 2014), influencing fault-zone architecture and potential fault reactivation (Dewhurst and Jones, 2003; Flodin et al., 2003; Wilson et al., 2006; Williams et al., 2016; Philit et al., 2019; Pizzati et al., 2019).

Granular or porous sediments and sedimentary rocks commonly contain sub-seismic-resolution strain localization features referred to as deformation bands (Aydin, 1978; DBs from now on). The effects of DBs on fluid flow can vary significantly depending on several factors, such as their permeability contrast relative to the host rock, their thickness, density, distribution, orientation, segmentation, and connectivity (Antonellini and Aydin, 1994; Gibson, 1998; Manzocchi et al., 1998; Sternlof et al., 2004; Shipton et al., 2005; Fossen and Bale, 2007; Torabi and Fossen, 2009; Rotevatn et al., 2013; Soliva et al., 2016). In some cases, DBs may act as conduits for fluids (Parry et al., 2004; Sample et al., 2006; Petrie et al., 2014; Busch et al., 2017). In most cases, however, they are associated with significant porosity and permeability reduction relative to the host rock (Antonellini and Aydin, 1994; Fisher and Knipe, 1998; Shipton et al., 2002; Sternlof et al., 2004; Balsamo and Storti, 2010; Ballas et al., 2015; Fossen et al., 2017; Del Sole and Antonellini, 2019), thus inducing permeability anisotropy and reservoir compartmentalization. This might negatively impact production from faulted siliciclastic systems (Edwards et al., 1993; Lewis and Couples, 1993; Leveille et al., 1997; Antonellini et al., 1999; Wilkins et al., 2019) and flow-based models and simulations (Sternlof et al., 2004; Rotevatn and Fossen, 2011; Fachri et al., 2013; Qu and Tveranger, 2016; Romano et al., 2020).

Cement has been found in association with DBs. Localization of cement along these structural features may significantly enhance porosity and permeability reduction caused by mechanical crushing and reorganization of grains, thus increasing their sealing or buffering potential (Edwards et al., 1993; Leveille et al., 1997; Fisher and Knipe, 1998; Parnell et al., 2004; Del Sole et al., 2020). The occurrence, distribution, and petrophysical properties of cement along DBs therefore need to be properly characterized and implemented into reservoir quality modeling to predict porosity, permeability, and their heterogeneity (e.g., Morad et al., 2010).

Models of calcite cementation, in particular, are fundamental for predicting sandstone and fault-rock properties such as porosity, permeability, compressibility, and seismic attributes. Diagenetic processes related to fluid flow mechanisms and evolution within DBs are not fully constrained; in particular, how DBs steer the origin and distribution of calcite cement remains poorly understood. Different processes account for enhanced fluid flow within DBs, such as unsaturated flow relative to the host rock in arid to semiarid vadose zones (Sigda et al., 1999; Sigda and Wilson, 2003; Wilson et al., 2003) and transient dilation in the early stage of DB formation (e.g., Antonellini et al., 1994; Main et al., 2000). Also, these mechanisms have been employed to explain the occurrence of cement and other processes (e.g., cementation, hydrocarbon inclusion entrapment, removal of iron oxide coatings) in and around the band (Fowles and Burley, 1994; Labaume and Moretti, 2001; Ogilvie and Glover, 2001; Parnell et al., 2004; Parry et al., 2004; Sample et al., 2006; Wilson et al., 2006; Cavailhes et al., 2009; Balsamo et al., 2012; Lommatzsch et al., 2015). These mechanisms, however, appear to be limited to specific conditions (e.g., cement precipitation in the early stage of DB formation or in vadose environments) assuming that DBs behave as fluid "conduits" in order to explain the occurrence of cement or other authigenic products within these structures. Nevertheless, a significant number of studies on DBs show that in most cases they are baffle or seals to fluid flow (see Ballas et al., 2015, for a review). Much less attention has been paid to fluid flow and diagenetic mechanisms leading to (post-DB formation) selective cementation in association with low-permeability baffle DBs (e.g., Philit et al., 2015), and models of cement precipitation in these DBs are limited to quartz cement and are mostly experimental (Lander et al., 2009; Williams et al., 2015). Different mechanisms, then, need to be invoked to explain the occurrence of (carbonate) cement in association with DBs in a broader set of conditions.

The aim of our work is to elucidate the influence of DBs on fluid flow and their role in fostering diagenesis and localizing diagenetic products in porous sandstones. The novelty of our work is that by using a multiscalar and cross-disciplinary approach integrating structural and diagenetic analysis, we assess the control exerted by DBs on flow pattern, the origin of diagenetic heterogeneities, and spatial distribution by means of the systematic characterization of the occurrence, as well as the spatial and microstructural relationship between DBs and cement nodules in two porous sandstone reservoir analogs. We examine two field sites in Italy and France where calcite cement nodules are spatially associated with DBs. The comparison between the two locations with different geological settings makes it possible to derive general conclusions that can be extended to other cases in which DBs and diagenetic processes interact. Our study also allows for the evaluation of the impact of both structural and

structural-related diagenetic heterogeneities on present-day fluid circulation and on subsequent deformation.

2 Geological framework

2.1 Loiano field site, northern Apennines (Italy)

The Loiano study area is in the northern Apennines (Emilia–Romagna region, Italy), 20 km to the south of the city of Bologna (Fig. 1a). The northern Apennines are an orogenic wedge formed in response to the upper Cretaceous–Eocene closure of the Ligurian–Piedmont ocean (Marroni et al., 2017) and the subsequent Oligocene–Miocene convergence and collision between the Adriatic Promontory and the Sardinia–Corsica Block of African and European origin, respectively (Vai and Martini, 2001). Our work focused on the Loiano Sandstones of the Epiligurian Successions (Fig. 1a–c), the middle Eocene to middle Miocene siliciclastic infill of thrust-top, piggyback basins discordant to the underlying Ligurian units, which migrated passively to the NE during the Apennines orogeny atop the entre orogenic wedge (Vai and Martini, 2001). The 300–1000 m thick, late Lutetian–Bartonian Loiano Sandstones are a fan delta to proximal turbidite deposit (Papani, 1998). They are medium- to coarse-grained, poorly consolidated, immature arkosic sandstones and conglomerates deposited in a relatively small lenticular basin (a few tens of kilometers in width and length; Fig. 1a, c). They are composed of 49 %–60 % quartz and 39 %–48 % feldspar, the rest being rock fragments, detrital carbonate clasts, and minor accessories (Del Sole and Antonellini, 2019).

2.2 Bollène field site, Southeast Basin (Provence, France)

The Bollène site is in the Southeast Basin of Provence (France), 15 km to the north of the city of Orange (Fig. 2a). The Southeast Basin is a triangular region between the Massif Central to the northwest, the Alps to the east, and the Mediterranean Sea to the south. It is a Mesozoic cratonic basin on the edge of the Alpine orogen, approximately 200 km long and 100 to 150 km wide. Three main tectonic episodes affected the region (Arthaud and Séguret, 1981; Roure et al., 1992; Séranne et al., 1995; Champion et al., 2000): SSW–NNE Pyrenean contraction from the Paleocene to Oligocene, NW–SE Gulf of Lion extension from the Oligocene to early Miocene (rifting), and, lastly, SW–NE Alpine contraction from the Miocene to Quaternary (Fig. 2a). The site of Bollène is exposed in a quarry (Fig. 2c) located in Turonian sand (low-cohesion sandstone) between 10 and 200 m thick and is situated north of the E–W Mondragon anticline (Fig. 2b, c). The Turonian sands at the Bollène quarry are laminated and fine- to coarse-grained with modal and bimodal grain size distributions; they formed in deltaic and eolian environments (Ferry, 1997). The host sands are not cemented. They are composed of 88 % to 92 % quartz, the rest being feldspar. The median grain diameter (D_{50}) is 0.31 mm, i.e., medium sand. Their porosities range from 20 % to 43 %, and the precise value at study site is 22 % (Ballas et al., 2014).

3 Methods

3.1 Outcrop analysis

The geometry and distribution of DBs and nodules were documented by detailed field mapping at different scales for both sites. At the Loiano site, a map (370 m^2) at the 1 : 25 scale (1 cm $\simeq$ 4 m) was made by standard topographic compass and tape mapping (Fig. 3). The Bollène quarry site pavement was mapped using a DJI PHANTOM™ drone. Photographs were taken at different heights above the ground surface and were then used to build a 3D mesh and extract high-resolution orthophotos using Agisoft PhotoScan Metashape software (© Agisoft LLC). The high-resolution orthophoto mosaic (1 px $\simeq$ 1–1.5 mm) was used for the detailed mapping of DBs and nodules. Furthermore, DBs and nodule patterns, as well as their characteristics and spatial relationships, were documented in the field on high-resolution photographs (15 megapixels) both in Loiano (Figs. 4 and 5) and Bollène (Figs. 7 and 8). Oriented samples were collected for thin section preparation, microstructural, and stable isotopes analysis. The orientation of DBs was measured at each site and plotted in lower-hemisphere equal-area stereograms, rose diagrams, and frequency histograms (Figs. 1d and 2d) using the Daisy3 software (Salvini, 2004).

3.2 Microstructural analysis

Polished thin sections of host sandstones, DBs, and nodules were analyzed by standard petrographic microscopy, cold cathodoluminescence, and backscattered electron imagery using a JEOL JSM-5400 and an FEI Quanta FEG 200 environmental scanning electron microscope (SEM). These microscopy techniques were used to examine the textural characteristics (e.g., grain size, shape, arrangements, contact relationships) and microstructures of host rock and DBs, as well as the cement distribution and texture (e.g., cement type and degree of cementation, cement crystal size and shape) (Figs. 9–11). In particular, cold cathodoluminescence (CL) analysis of carbonate cement in nodules was conducted with a CITL cold cathodoluminescence 8200 Mk5-1 system (operated at 14–15 kV beam energy and 250 µA beam current) equipped with a standard petrographic microscope (Olympus BH41). CL was used to describe the cement crystal properties (texture, fabric, luminescence) and the micron-scale spatial distribution and textural relationship among the cements, framework detrital grains, and fractures (sensu lato). This information is used to (i) understand the interrelation between deformation, fluid flow, and diagenesis (e.g., cement precipi-

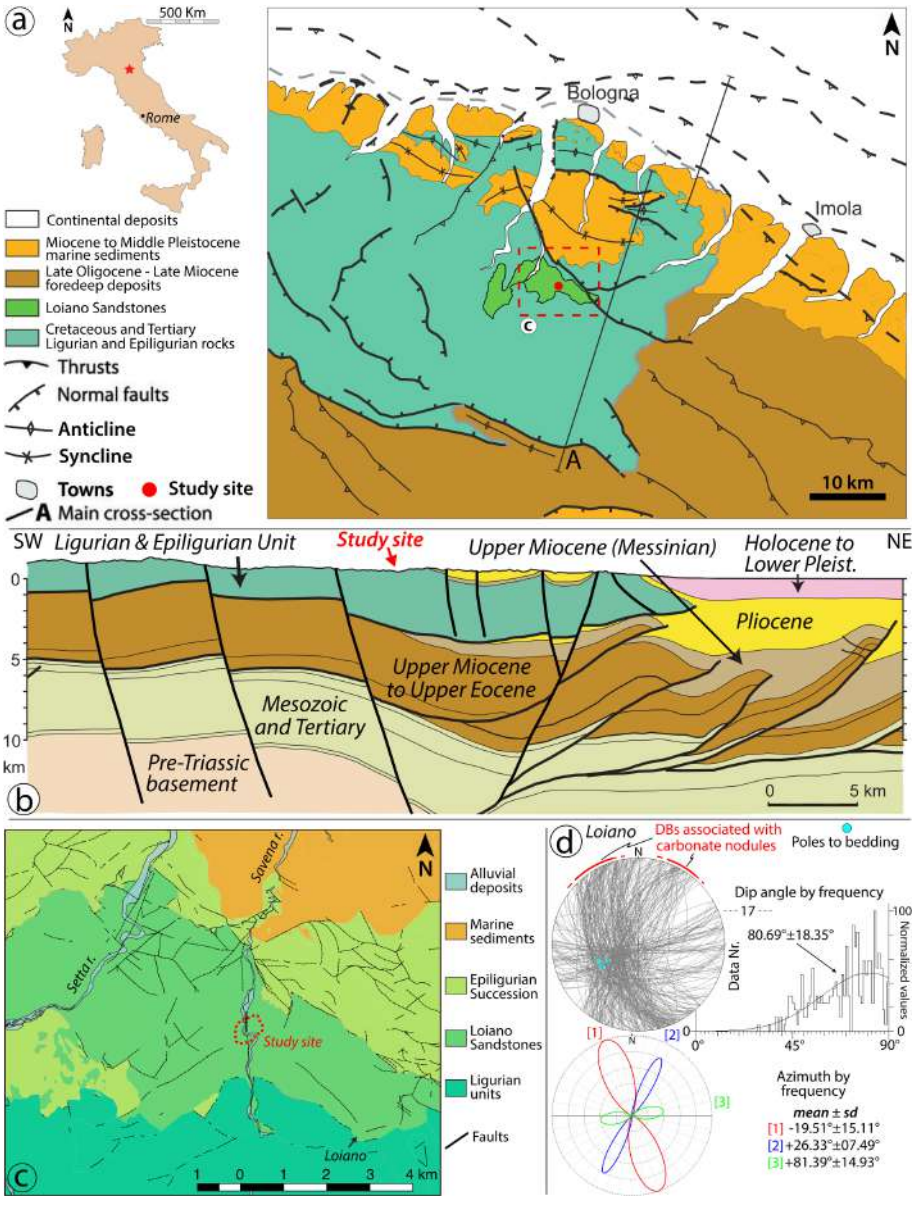

Figure 1. **(a)** Schematic geologic map and **(b)** cross section of the northern Apennines near Bologna (Italy), modified from Picotti and Pazzaglia (2008). **(c)** Geologic map of the study area and location of the studied outcrops (red dotted line). This map is constructed from data on the Regione Emilia–Romagna (http://www.regione.emilia-romagna.it/, last access: 17 December 2019). The location of **(c)** is indicated by a red square in **(a)**. **(d)** Lower-hemisphere equal-area projection indicates the orientation of the different sets of DBs (298 data points) and poles to bedding at the study site. DBs associated with carbonate nodules are highlighted by a red line. DBs azimuth (strike; $N \pm 90°$) frequency rose diagram and dip angle (°) plotted against frequency. Best-fit Gaussian curves superimposed on the corresponding data histograms (frequency distributions). Gaussian peaks and related standard deviations (±SD) are indicated for each population.

tation); (ii) assess the relative timing of each process; (iii) describe porosity evolution with time; and (iv) understand the mechanisms and the geochemical environment of cement precipitation when coupled with other tools (e.g., stable isotopes analyses). The CL features (color, brightness) of the carbonate minerals are controlled primarily by the relative abundances of Mn^{2+}, REEs, and Fe^{2+}. These differences, in turn, reflect specific physiochemical conditions of formation waters during mineral growth, including fluid chemistry (salinity), pH and Eh, temperature, pressure, ion activity, and biological activity (e.g., Marshall, 1988; Barnaby and Rimstidt, 1989; Machel, 2000; Hiatt and Pufahl, 2014).

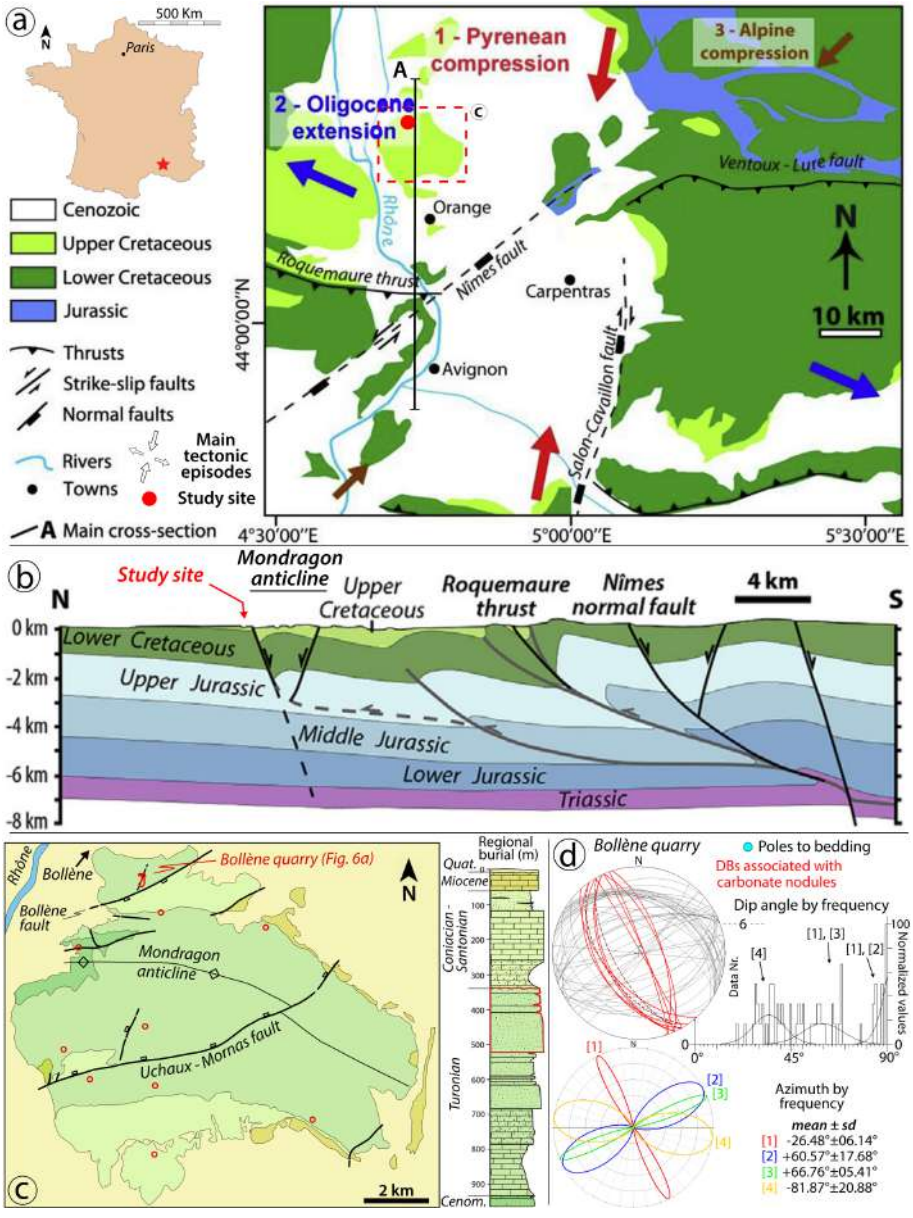

Figure 2. **(a)** Schematic geologic map and **(b)** cross section of the Southeast Basin, Provence, France. The main tectonic episodes affecting the region are reported in **(a)**. **(c)** Geologic map and stratigraphic column of the Bollène quarry. The location of the map in **(c)** is indicated by a red square in **(a)**, and red open circles indicate some past study locations (see Wibberley et al., 2007; Saillet and Wibberley, 2010; Ballas et al., 2012, 2013, 2014; Soliva et al., 2013; Philit et al., 2018). Panels **(a)** and **(b)** as well as the stratigraphic column in **(c)** are modified from Philit et al. (2015, 2018). The geological map in **(c)** is modified from Ballas et al. (2012). **(d)** Lower-hemisphere equal-area projection indicates the orientation of the different sets of DBs (64 data points) at the study site. DBs associated with carbonate nodules are highlighted in red. Dotted lines indicate the main attitude of tabular carbonate nodules. DBs azimuth (strike; $N \pm 90°$) frequency rose diagram and dip angle (°) plotted against frequency. Best-fit Gaussian curves superimposed on the corresponding data histograms (frequency distributions). Gaussian peaks and related standard deviations (±SD) are indicated for each population. The numbers in square brackets [n] are the same as used in Fig. 6b to rank different sets of DBs.

3.3 Stable isotope characterization

Stable carbon and oxygen isotope data from cements from within carbonate nodules were used to constrain the geochemical environment of precipitation and possible source of fluids. Powder samples for bulk rock carbon and oxygen stable isotopes analysis were ground with a dental drill from unweathered or altered sections of the nodules. A total of 46 sites were sampled from nodules in Loiano ($n = 30$; Fig. 12a) and Bollène ($n = 16$; Fig. 12b). Powders samples were ana-

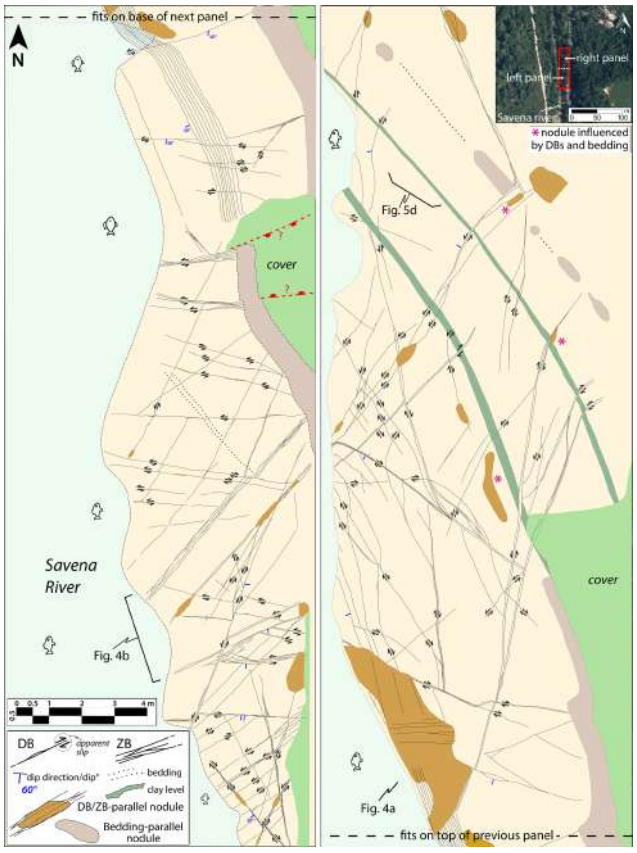

Figure 3. Outcrop map that documents the geometry and distribution of DBs and nodules in a portion of the study area in Loiano. The right-hand panel fits on top of the left-hand panel. ZB – zone of bands. The inset (© Google Earth) shows the map location in the study area.

lyzed with a Thermo Finnigan DELTA plus XP mass spectrometer coupled with a Thermo Finnigan Gas Bench II gas preparation and introduction system. $\delta^{13}C$ and $\delta^{18}O$ refer to the international standard VPDB (Vienna Pee Dee Belemnite). Isotope determination analytical precision was 0.10 ‰ and 0.15 ‰ VPDB for carbon and oxygen, respectively. The uncertainty was ca. 0.15 ‰ for carbon and ca. 0.20 ‰ for the oxygen isotopes.

4 Deformation bands and cement: field observations

4.1 Loiano

At the study site, bedding strikes NW–SE and dips at an average of 38° to the NE (Fig. 1d). Deformation bands cluster into three different trends striking 340° (NNW–SSE), 26° (NNE–SSW to NE–SW), and 81° (ENE–WSW) (Fig. 1d). All DBs dip moderately to steeply, mostly in the west and south quadrants (Fig. 1d). Deformation bands commonly occur with a positive relief and appear as whitish linear traces with minor undulations forming eye and ramp structures, whereby they branch and merge (Figs. 3 and 4). Already at the outcrop they exhibit a significant reduction in grain size and porosity in comparison to the surrounding host rocks (Fig. 4f). Deformation bands occur both as single features and as clusters or zones of bands, i.e., in narrow zones with variable thickness (0.8–60 cm) with subparallel DBs (up to 40). Single DBs accommodate minor offsets from a few millimeters up to 40 mm, whereas clusters can accommodate offsets up to 0.5 m (Fig. 4b, d). Deformation bands display a variety of apparent normal and strike-slip offsets (Fig. 3). Different sets of DBs show ambiguous and conflicting crosscutting relationships. Field observations indicate that the NNW–SSE and NNE–SSW sets have mutual crosscutting relationships typical of faults forming synchronously (Fig. 3).

The peculiar characteristic of the Loiano Sandstones is the occurrence of spatially heterogeneous carbonate cement in the form of isolated or multiple spheroids or irregular nodules and continuous tabular nodules (Figs. 4 and 5). The nodules weather out in positive relief because they are more resistant to weathering than the weakly cemented host rock. Isolated nodules range in diameter (major horizontal axis) from 0.2 to 3 m (Fig. 4c, d), whereas tabular concretions have a thickness ranging from 0.10 to 0.8 m and a long axis ranging from 3 up to 15 m in length (Fig. 5a). Generally, the nodule shape in Loiano is similar to that of an oblate spheroid. There is no evidence of spherical nodules or prolate spheroids. The volume of the carbonate nodules ranges from 0.001 m^3 to > 10 m^3. Nodules form about 20 % of the exposed outcrop volume. Two types of nodules can be distinguished depending on whether they are associated with DBs and/or clusters (i.e., DB-parallel nodules; Figs. 3, 4, and 5a–c) or with bedding planes (i.e., bedding-parallel nodules; Figs. 3 and 5d, e). The former represent roughly 75 % of the total nodules in the study area and are the main target of this work. The association between DBs and nodules occurs in the form of (i) parallelism and spatial overlap between DBs and nodules and (ii) confinement of the nodules by the DBs. In all cases, nodules are oriented with the major axis (elongation direction) parallel to the DBs and the minor axis (i.e., thickness) perpendicular to them. Deformation-band-parallel nodules are isolated ellipsoids (Fig. 4b, d) or, alternatively, continuous tabular objects (Figs. 4a and 5a). Nodules may be located along the DB (or zone of bands) trace (Figs. 4a, d and 5a, b), placed in between, and confined by DBs (Figs. 4b, e, and 5c), or they may be asymmetrically placed on one side of the DBs (Figs. 4c and 9e). In some cases, nodules lie at the intersection of different DB planes (Fig. 3). Some DBs are not spatially associated with nodules (Figs. 3 and 4b). Among the multiple sets of DBs, those mostly associated with carbonate nodules are the NNW–SSE and the NNE–SSW ones. As a result, most nodules are elongated along these two structural directions (Figs. 1d and 3; see also Fig. 1b in Del Sole and Antonellini, 2019). The other

Figure 4. Relationships between nodules and DBs. Deformation bands occur either as single structures or organized in clusters (ZB). Nodules along DBs (or ZB) are isolated **(b, d, e)** or continuous with a tabular geometry **(a)**. Nodules are located along the DB trace **(a, b, d)**, or they are asymmetrically placed on a side of the DB **(c)**. **(e)** Isolated nodule in between and confined by ZB. DBs are whiter than host rock and exhibit a positive relief, a clear reduction in grain size, and a lower porosity visible to the naked eye **(f)**. The pen in **(c, d)** is 14 cm in length. The arrow scale in **(b, e)** is 10 cm in length. The position of **(a, b)** is indicated in Fig. 3.

sets are rarely associated with carbonate nodules. Nodules are never cut across by the DBs.

Bedding-parallel nodules are either isolated (Fig. 3) and multiple but laterally discontinuous (Figs. 3 and 5d, e) or laterally continuous layers with a tabular geometry (Fig. 3; e.g., "nodular beds" in Del Sole et al., 2020). Nodular beds are continuous pervasively cemented layers that extend along the bedding plane for several meters (up to 15 m in length) with a nearly constant thickness of ca. 35–50 cm. Nodules along bedding planes are more rounded gentle boundaries (Fig. 5d, e) than those associated with DBs, which are instead more tabular and exhibit angular and sharp boundaries (Figs. 4 and 5a–c). In some cases, nodule geometry and elongation direction follow both bedding surfaces and DBs (Fig. 3). Nodules, despite being ubiquitous in the sandstone, are mostly observed within coarse levels with a grain size equal to or larger than medium sands (0.25–0.5 mm). We did not observe any nodules in sedimentary rocks with a grain size finer than sand (siltstone and clay). Bedding-parallel nodules are commonly located in sandstone levels confined between clay–silty levels or fine-grained sand levels (Figs. 3 and 5d, e).

A set of joints and veins (Fig. 5a, b) was found exclusively within the carbonate nodules. They postdate DBs and nodules and do not propagate into the surrounding host sandstone.

4.2 Bollène

At Bollène, DBs occur as belonging to three different trends oriented (i) NW–SE to NNW–SSE (set 1: 334°; Figs. 2d and 6b), (ii) NE–SW to ENE–WSW (set 2: 61° and set 3: 67°; Figs. 2d and 6b), and (iii) ESE–WNW (set 4: 278°; Figs. 2d and 6b). Trend (i) can be divided into two subsets; one is characterized by normal offset NW–SE conjugate bands with moderate dip angles (50–60°) to SW (Figs. 7a and

Figure 5. **(a–c)** DB-parallel- and **(d–e)** bedding-parallel nodules. **(a)** Decametric-scale continuous nodule with a tabular geometry located along a zone of bands (ZB). NE-dipping layering is shown with dotted lines. The photo is about 10 m in depth. **(b)** Close-up of **(a)** from a map view. The lens cover is 5.5 cm in diameter. **(a, b)** Late-opening fractures cut through the assemblage "DBs – nodule" and they do not propagate into the poorly consolidated host rock. **(c)** Isolated nodules placed in between and confined by ZB. **(d, e)** The bedding is emphasized mostly by clay and silt horizons, sporadic well-defined thin levels of gravel, and the alignment of bedding-parallel nodules. **(d)** Black arrows point to multiple but laterally discontinuous bedding-parallel nodules. Here, a single DB (white line) crosses a bedding-parallel nodule without causing any offset. The position of **(d)** is indicated in Fig. 3. **(e)** Photomosaic showing a series of laterally discontinuous nodules just below, above, or in between several continuous impermeable clay-rich levels. The deformation pattern changes depending on the host rock properties (e.g., sorting degree, porosity ϕ, grain size; see Supplement S1 for details). Cataclastic deformation is accompanied by clay smear (see inset) whereby DBs cut thin dark-colored clay levels.

8a, c) and just a few to NE; a second one is characterized by dominant dextral strike-slip kinematic bands with higher dip angles (70–90°) and a NNW–SSE trend (Figs. 6b and 7f). Trend (ii) can be divided into two sets; one set is characterized by dominantly left-lateral and minor right-lateral subvertical strike-slip conjugate bands striking NE–SW to ENE–WSW (set 2 in Fig. 6b; Fig. 7a–c); a second set is instead characterized by a set of conjugate DBs with moderate dips ($\sim 60°$), NE–SW orientation (set 3 in Fig. 6b), and undetermined kinematics (likely normal-sense). Trend (iii) is com-

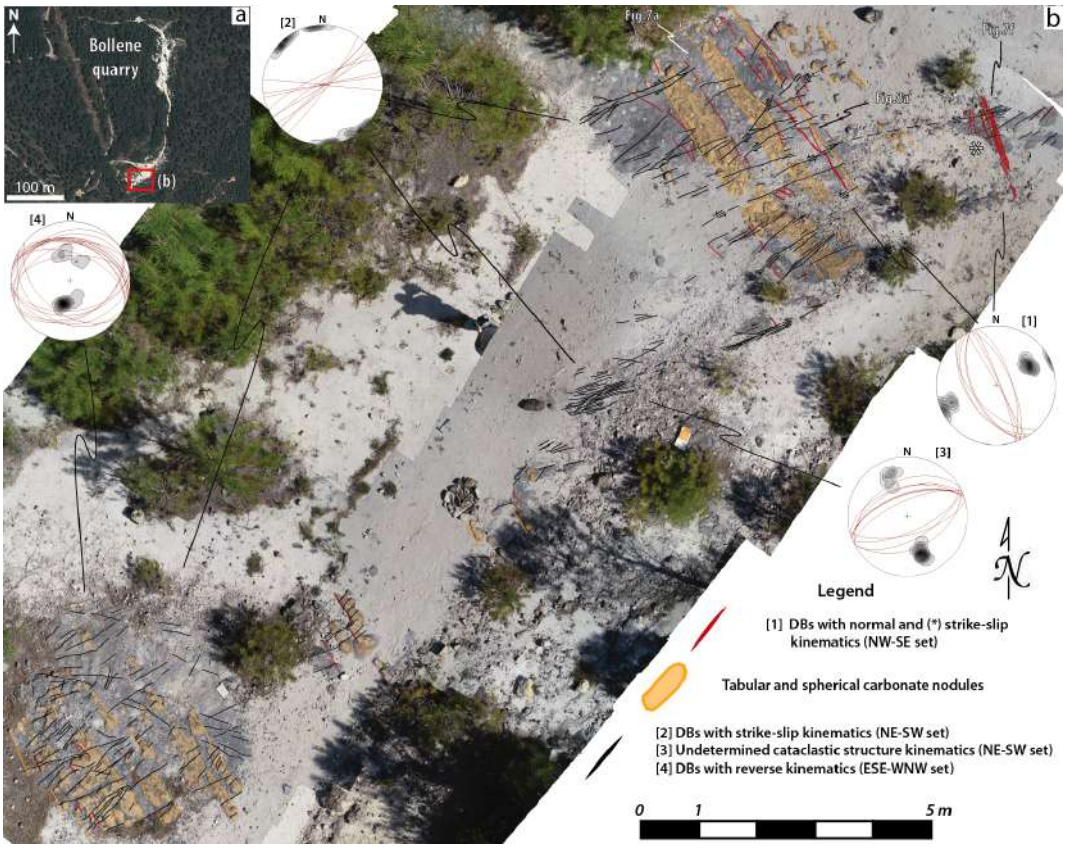

Figure 6. **(a)** Aerial photograph of the study site (© Google Earth). **(b)** Orthophoto that documents the geometry and distribution of DBs and carbonate nodules in the Bollène quarry. Lower-hemisphere equal-area projection indicating the orientation of the cataclastic structures measured in (1) NW–SE/NNW–SSE normal and (dextral) strike-slip bands associated with tabular and spherical nodules; (2) NE–SW/ENE–WSW strike-slip bands; (3) NE–SW bands with undetermined kinematics; (4) ESE–WNW reverse-sense bands.

posed of ESE–WNW conjugate bands, with reverse kinematics and low dip angles (30–40°). In the field, DBs appear as whitish linear traces with minor undulations and characteristic eye structures whereby they branch and merge (Figs. 6b and 7). In most cases, DBs weather out in positive relief. Frequently, DBs occur in narrow zones (a few millimeters up to 5–15 cm in thickness). Field observations indicate that ESE–WNW DBs are crosscut by NE–SW strike-slip DBs (Fig. 6b). The latter also crosscut the NW–SE/NNW–SSE set (Fig. 7a–c, f). Bedding is oriented NW–SE and dips gently ($< 10°$) to the S (Fig. 2b, d). Bedding is difficult to recognize on the floor of the quarry because of its low dip and the massive texture of the rock (Fig. 6b). The Turonian Sandstones outcrop on the quarry floor. There are two lithotypes. The first one is represented by massive porous sands with DBs and localized carbonate cementation (see description below). The second one is characterized by a massive calcrete level with tabular geometry (see Supplement S2 for details).

The Turonian Sandstones in the Bollène quarry are characterized by a spatially heterogeneous cementation (Fig. 6b). These diagenetic heterogeneities occur as spherical and tabular nodules (Figs. 7 and 8). Spherical nodules are arranged as isolated bodies within the surrounding host rock (Figs. 7c, g and 8a, d, e) or aggregated in tabular clusters (Fig. 7a, d). Nodules weather out in positive relief. Spherical nodules range in diameter from a few millimeters (0.004–0.005 m) to a few tens of centimeters (0.2 m), whereas tabular ones have a thickness ranging from a few centimeters to 0.1 m and a long axis up to 5 m in length (Figs. 6b and 7a–c). Assessment of the nodule lateral extension is hampered by the presence of vegetation and debris cover, whereas subsurface extension cannot be measured because of the limited vertical exposures of the outcrops. Hence, the values reported here are minimum values. In general, the nodule shape may be approximated by a sphere for which length, width, and thickness are "equal" and by an oblate spheroid for which length and width are larger than the nodule thickness. Carbonate nodule volume ranges from 10^{-7} (small spherical nodules) to $> 2.5\,m^3$ (tabular nodules assuming length and width of 5 m and thickness of 0.1 m). In Bollène, the nodules are all spatially and geometrically associated with DBs (i.e., DB-parallel nodules; Figs. 6b and 7). This association occurs in the form of (1) parallelism between DBs and nodules, (2) geometric congruence between the DB trend and

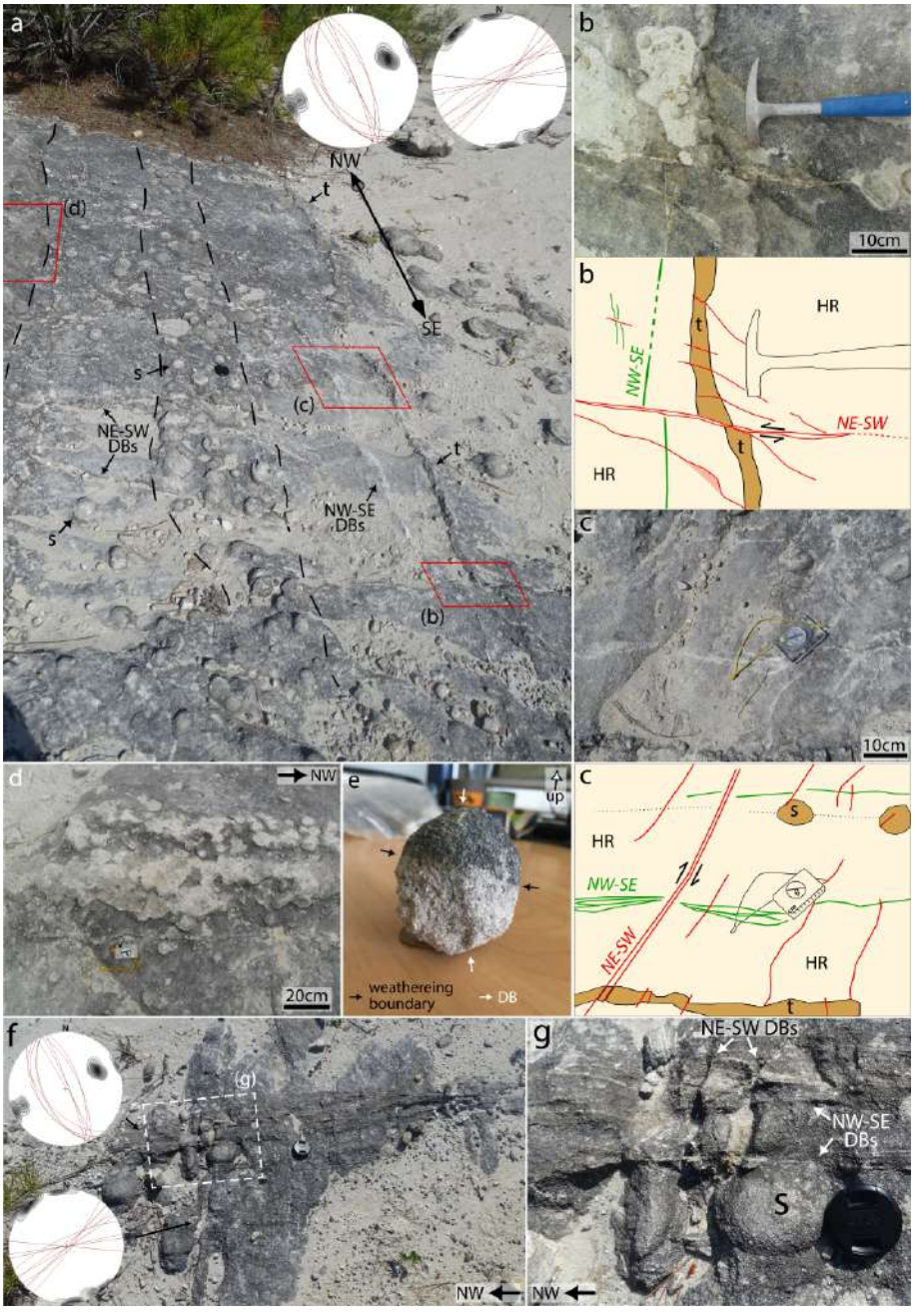

Figure 7. Calcite cement occurs isolated **(a, c, g)** or in clusters **(a, d)** of (S) spherical nodules and continuous (t) tabular nodules **(a–c)**. Nodules are arranged in compartments parallel to clusters of NW–SE normal bands **(a–c)** and to NNW–SSE dextral strike-slip bands **(f, g)**. NE–SW/ENE–WSW strike-slip bands displace both the NW–SE bands and their associated nodules **(a–c, f)**. **(e)** Spherical nodule (about 5 cm in diameter) in spatial superposition with a NW–SE DB that does not displace the cement. The lens cover in **(a, f)** has a 5.5 cm diameter. The figures **(a–d, f, g)** are in map view. The position of **(a, f)** is indicated in Fig. 6b. Hammer length in **(b)** is 30.5 cm.

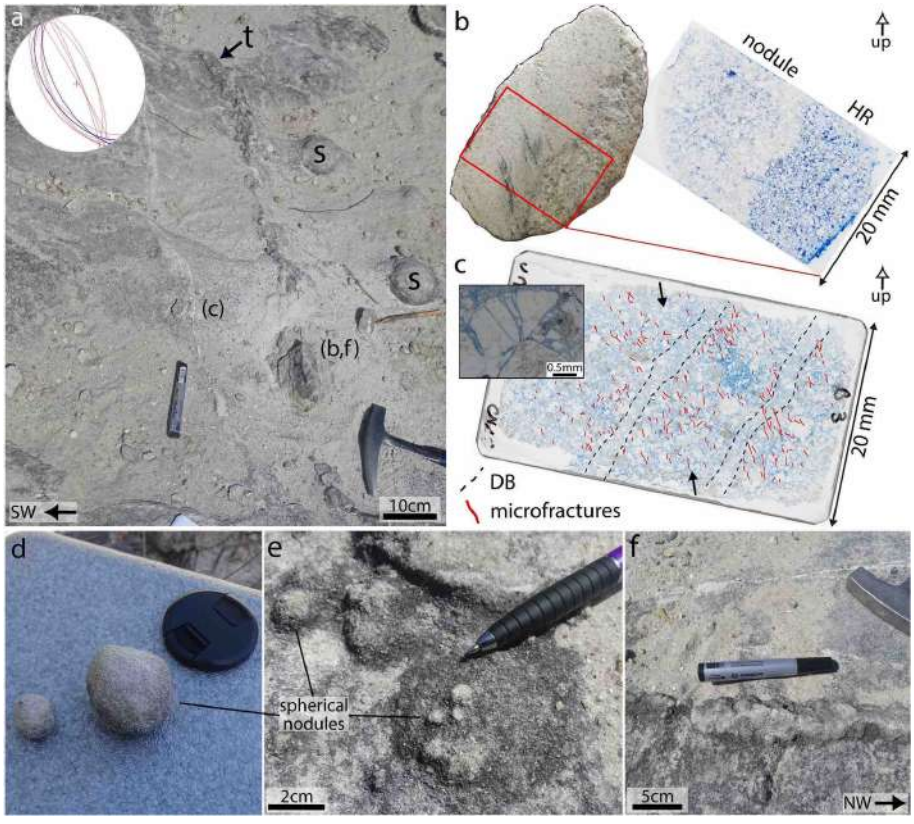

Figure 8. Typical relationships between nodules and DBs. **(a)** Continuous tabular nodule (t) and isolated spherical nodules (S) aligned parallel to the NW–SE normal-sense bands dipping SW (∼ 55°; red lines in the inset stereoplot). The tabular bodies dip to the SW parallel to the bands (blue lines in the stereoplot in the inset). The position of **(a)** is indicated in Fig. 6b. **(b)** Hand specimen and polished thin sections impregnated with blue-dyed resin of a tabular nodule in **(a)**. **(c)** Polished thin sections impregnated with blue-dyed resin showing two subparallel NW–SE normal-sense bands dipping SW. Mapping of microfractures developed at grain contacts consistent with Hertzian contacts (e.g., Eichhubl et al., 2010; Soliva et al., 2013) endorses the normal kinematic of these bands (see Supplement S1 for details). "Up" refers to the topography. Close-up of spherical **(d–e)** and tabular **(f)** nodules from the field. Pen and marker length in **(a, f)** is about 13.5 cm. The lens cover in **(d)** has a 5.5 cm diameter.

the nodule (or nodules cluster) shape, and (3) confinement of nodules in parallel-to-band compartments. In all these cases, tabular nodules and clusters of spherical nodules are oriented with the major axis (elongation direction) parallel to the DBs and the minor axis (i.e., thickness) perpendicular to them (Figs. 7a and 8a). Unlike what we have seen in Loiano, in Bollène nodules are in compartments among DBs. Carbonate nodules are associated with the NW–SE/NNW–SSE DB set (Figs. 6b and 7a, f). Although this set is conjugate with bands dipping to the SW and to the NE, the tabular cement bodies dip only to the SW (Figs. 2d and 8a–c). No nodules are cut by the NW–SE bands. The NE–SW/ENE–WSW strike-slip bands cut through the NW–SE/NNW–SSE bands and the associated NW–SE-trending carbonate nodules (Figs. 7a–c, f). There is clear evidence of these crosscutting relationships both at the outcrop and at the microscale (see Sect. 5.2). For this reason, we focus on the NW–SE DBs and nodules in the remaining part of this study.

5 Deformation bands and cement: textural and microstructural characteristics

5.1 Loiano

Host rock total porosity (minus cement ϕ) is between 20 % and 26 % (Fig. 9; Del Sole and Antonellini, 2019). Porosity is predominantly intergranular, whereas intragranular (e.g., pores within bioclasts) and "oversize" pores are due to dissolution of detrital grains (Figs. 9 and 10). Deformation band total porosity (minus cement ϕ) is lower by an order of magnitude (below 5 %) than the host rock porosity (Fig. 9d). In the nodules, the host rock porosity is almost completely filled by cement (Fig. 10) so that the remnant porosity (voids) is low (down to 1.3 %) (Fig. 9a, c). The presence of cement within the DBs enhances the porosity reduction caused by grain crushing and compaction (Fig. 9d). The microstructure of the DBs is characterized by reduced grain size, porosity, and pore size compared to the host rock (Fig. 10i–l). Within

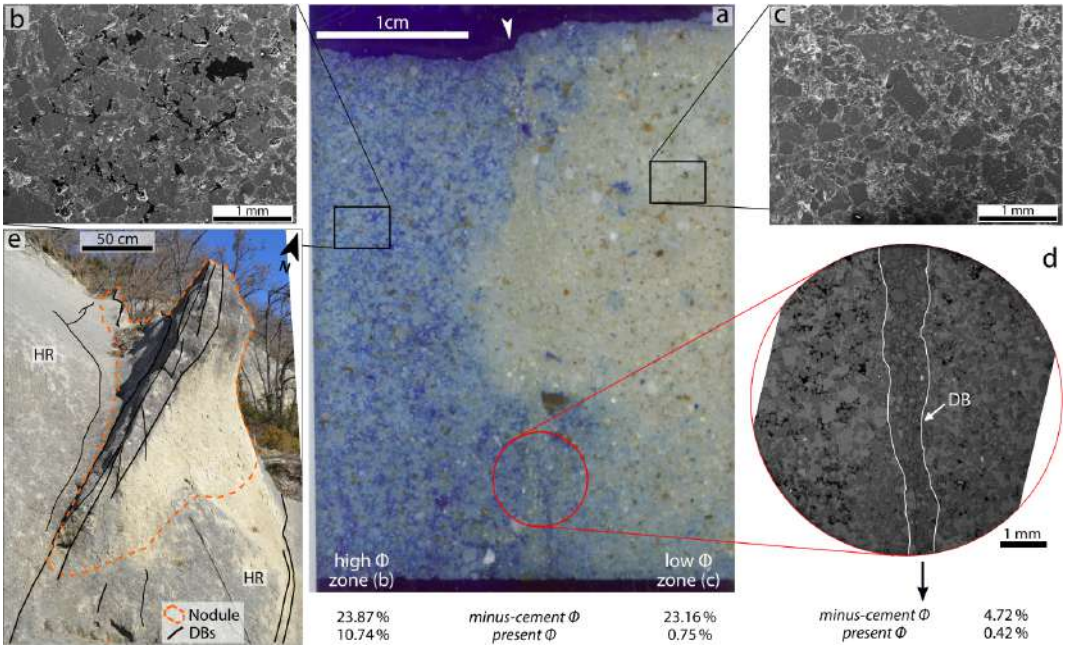

Figure 9. Host rock (HR) and DB porosity as well as relationships between cement and DBs in the Loiano Sandstones. **(a)** Polished thin sections impregnated with blue-dyed resin. The section shows a DB (arrow) separating two host rock sectors: on the right-hand side there is extensive calcite cementation, whereas on the left-hand side cementation is poor. **(b, c)** Secondary electron and **(d)** backscattered electron SEM images from different sectors of the section **(a)**. Porosity (ϕ) estimation data in **(a–d)** are from Del Sole and Antonellini (2019). **(e)** Field example for which a nodule is asymmetrically placed on a side of the DBs, similarly to what is observed in **(a)**. See text for further details.

the DBs a few coarse grains are surrounded by a fine-grained matrix.

Despite the different effects of mechanical and chemical compaction as well as minor authigenic alterations (refer to Supplement S1 for details), the major diagenetic components of the Loiano Sandstone are calcite cements. These cements fill mainly intergranular, and to a lesser extent intragranular (intraskeletal), pore spaces and intragranular fractures, and they encase the framework grains and all other diagenetic features. Bedding-parallel nodules (Fig. 10a–h) are characterized by a mosaic texture of blocky sparite to poikilotopic bright-orange to orange CL calcite cement. Crystal size is typically 40–100 µm and up to 300 µm (Fig. 10g, h). This cement phase is the most widespread one and it is uniform almost everywhere in terms of texture and CL pattern, if not for some minor dark CL subzones (Fig. 10g, h). A minor calcite cement phase is associated with detrital carbonates (bioclasts) and it shows a bright-orange CL (Fig. 10c–d). It occurs as pore lining formed by elongate and sharp rhombohedral calcite (dogtooth) that outlines the outer rim of the bioclasts (Fig. 10c) and drusy mosaic calcite that fills intraskeletal pores, outlines bioclasts, and fills intragranular fractures in bioclasts (Fig. 10d). This subordinate phase was observed only in bedding-parallel nodules. Pore-lining cement around bioclasts is present only where there was pore space (now filled), whereas it is absent where other grains are in contact with the bioclast. All cement phases described above (intergranular, intraskeletal, and pore lining) encase compacted grains, and cements are undeformed, still preserving the original shape. Pore-filling cement in DB-parallel nodules (Fig. 10i–n) shows a similar texture and CL pattern as that described for the main intragranular cement phase in the bedding-parallel nodules (Fig. 10a–h). The main features that differentiate DB-parallel nodules from bedding-parallel ones are the finer crystal size of calcite within DBs (Fig. 10i–l) and the absence of a bright-orange CL cement phase described in association with bioclasts in bedding-parallel nodules (Fig. 10c, d). Some bright-orange CL cement was observed only in detrital form (crushed) within the DB (Fig. 10k). The pore filling in DBs is fine-grained sparite; no evidence was found of crushed calcite crystals belonging to the dominant calcite phase. The finer fraction within the DBs is a matrix made up of comminuted angular and fine-grained clasts (flakes) of feldspar and to a smaller degree quartz, encased by the cement (Fig. 10j–l). Similarly, the cement fills the microfractures that cut through coarser grains and it encase the fine-grained clasts that are present within these fractures. Although these microfractures are frequent in the host rock sectors in proximity to the DB (Fig. 10i), they were also observed in bedding-parallel nodules (Fig. 10a, b). Host rock volumes within DB-parallel nodules are still characterized by blocky sparite cement with some minor dark CL growth subzones (Fig. 10i, m, n), similar to what was observed in bedding-parallel nodules.

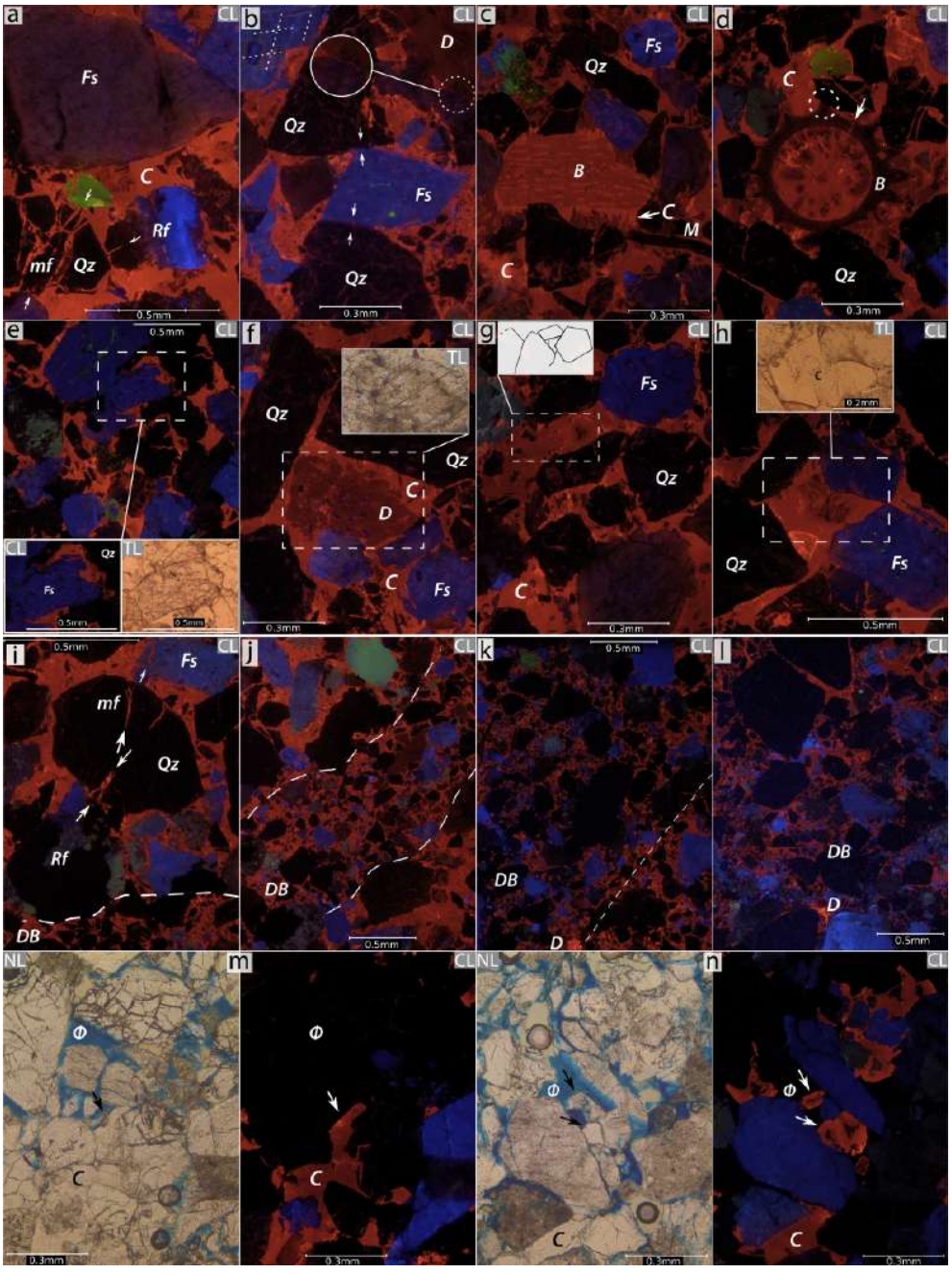

Figure 10. Natural- and CL-light photomicrographs showing the microstructure and cement textures in **(a–h)** bedding-parallel and **(i–n)** DB-parallel nodules. **(a–b, d)** Microfractures form at grain contacts due to stress concentration at contact points, and **(i)** they are common in the host rock areas close to the DB. **(b)** Feldspars break mainly by cleavage-controlled intragranular fractures (white dotted line). Some framework grains show planar to slightly undulated framework grain-to-grain contacts. Detrital carbonate clasts and **(c–d)** bioclasts are partially dissolved at grain contacts. **(e)** Some detrital grains are corroded and coated or partially replaced by cement. **(f)** Syntaxial overgrowth cement on a detrital carbonate clast (D). Bright CL **(c)** circumgranular pore lining (dogtooth texture) and **(d)** intraskeletal (drusy mosaic) calcite cement were observed only in bedding-parallel nodules. The main cement phase is characterized by bright-orange to orange CL calcite cement that fills intergranular porosity and intragranular fractures both in **(a, b, e–h)** bedding-parallel nodules and **(i–n)** DB-parallel ones. **(g–h, m–n)** Host rock volumes in nodules are characterized by blocky sparite to poikilotopic calcite cement with minor dark CL subzones, whereas **(j–l)** the cement in DBs is fine-grained sparite. **(m–n)** At nodule edges, cement crystal rims are regular and sharp, suggesting absent or negligible dissolution. Bright grains in **(k, l)** are detrital calcite (D). Qz – quartz; Fs – feldspar; M – mica; Rf – rock fragment; B – bioclast; ϕ – pore space; C – calcite cement; TL – transmitted light. See text and Supplement S1 for further details.

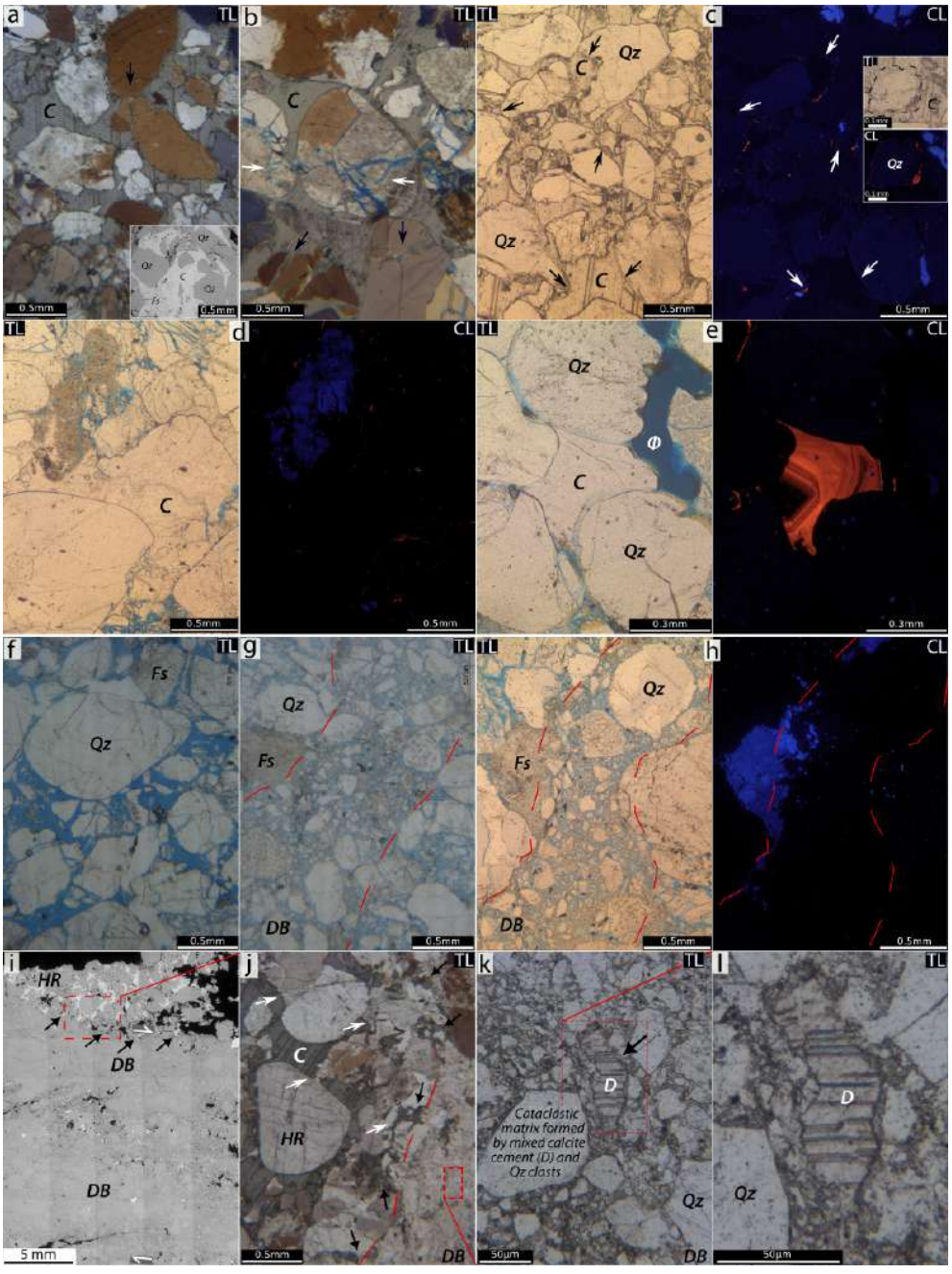

Figure 11. Natural- and CL-light photomicrographs showing the internal texture and microstructure of **(a–e)** spherical and tabular nodules and **(f–l)** DBs. **(a, b, f)** Host rock grains are mostly rounded and nearly undisturbed. Some microfractures break framework grains at contact points. In nodules, **(a)** some of the microfractures are filled; **(b)** a few are not. **(g, h)** Microfractures are more frequent approaching the DB, and **(j)** they are preferentially oriented with respect to the band (white arrows). Cement fills intergranular pore space and intragranular fractures. **(c–e)** The major diagenetic component is poikilotopic spar cement with dominant dark luminescence and **(e)** minor bright-orange CL growth subzones. **(c)** A very thin film of bright-orange CL calcite cement often coats detrital grains. Minor diagenetic alterations are corroded detrital grains that are partially replaced by calcite cement; see inset in **(c)**. **(g, h)** NW–SE bands and **(i, l)** NE–SW strike-slip bands show a similar pattern, but NE–SW bands feature a high degree of grain comminution and porosity reduction. **(i, j)** NE–SW strike-slip bands crosscut cement nodules; intragranular fractures (white arrows) and incipient stage of cement comminution (black arrows) between quartz clasts in the host rock sectors in proximity to these bands. **(k, l)** Fine particles of crushed detrital calcite cement (D) are found among the matrix grains at the crosscutting site. The inset in **(a)** is a backscattered electron SEM image. Qz – quartz; Fs – feldspar; ϕ – pore space; C – calcite cement; TL – transmitted light. See Supplement S1 for details.

To evaluate any sign of dissolution in nodules, we carefully checked cement crystal morphologies adjacent to poorly cemented or non-cemented host rock sectors at the edges of nodules. Here, cement crystal boundaries are regular and sharp (Fig. 10m, n).

5.2 Bollène

The host sands at Bollène are weakly cemented, with the exception of localized carbonate cementation described above. Host rock grains are mostly rounded and lack a fabric (Fig. 11a, f). Here, we describe the microstructure of NW–SE/NNW–SSE normal-sense and strike-slip bands, as well as NE–SW/ENE–WSE strike-slip bands sets. The most recognizable features that characterize both DB sets are the reduction of grain size and porosity, as well as a tighter packing relative to the host rock (Fig. 11). NE–SW strike-slip bands (Fig. 11i–l) have a higher degree of grain comminution, porosity reduction, and tighter packing when compared to NW–SE bands (Figs. 8c and 11g–h). Most grains within the bands are fractured and angular. Despite the strong comminution, a few rounded large survivor quartz grains are preserved in the DB matrix (Fig. 11g, h, k). Fine angular grains that are mostly comminuted feldspar fragments and secondary quartz and minor oxides make up the matrix. We also observed fine particles of crushed calcite cement among the matrix grains within NE–SW bands (Fig. 11k, l). In some cases, the grains in the host rock areas in proximity to the DB are encased by relatively undeformed carbonate cement (Fig. 11i, j). Some grains in the host rock are corroded and partially replaced or coated by calcite cement (Fig. 11c).

The main cement in spherical and tabular nodules is a poikilotopic calcite that infills intergranular pores (Fig. 11a–e). Most of the cement is non-luminescent (dark luminescence) under CL (Fig. 11c, d), but a few crystals show partial overgrowths with a bright-orange CL color (Fig. 11e). When the crystal has a heterogeneous CL pattern, the non-luminescing zones are mainly in the crystal core, whereas the luminescing subzones are mostly at the crystal edges (Fig. 11e). A very thin film (up to ca. 10 µm thick or less) of bright-orange CL calcite cement commonly coats the detrital grains (Fig. 11c), and it is also visible under natural light (Fig. 11b). In the nodules, some of the intragranular microfractures at contact points are filled by cement (Fig. 11a); a few are not (Figs. 11b). The cements described above (pore filling and grain coating) are relatively undeformed (i.e., no microfractures, no twin lamellae) and still preserve the original shape, except where the NE–SE/ENE–WSW strike-slip bands crosscut the cement nodules. At the crosscutting site, indeed, and more specifically in the host rock sectors in proximity to the NE–SW/ENE–WSW bands, we observe intragranular fractures at contact points and the onset of cement comminution between quartz clasts (Fig. 11i, j). Fine particles of crushed detrital calcite cement are found among the cataclastic matrix grains within NE–SW/ENE–WSW strike-slip bands where they interact with nodules (Fig. 11k, l). At the microscale, no preferential or significant calcite cementation was observed in association with the NW–SE bands. The association between cements and these latter bands was observed only at the mesoscale (see Sect. 4.2).

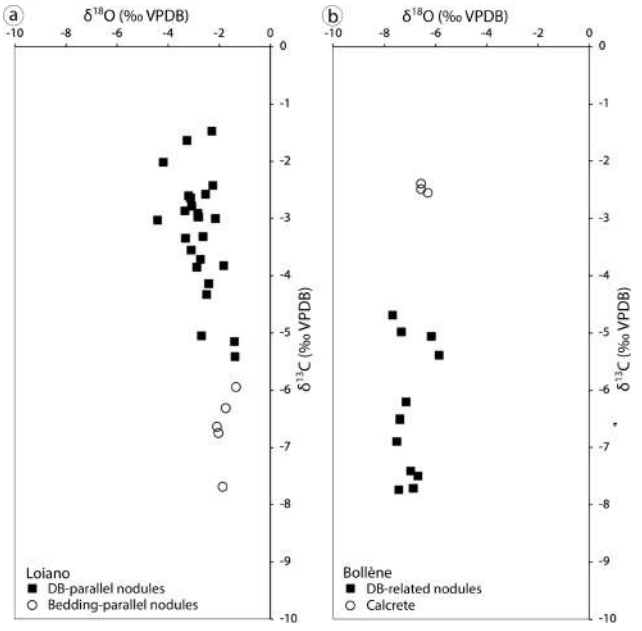

Figure 12. Stable isotope analysis results. **(a)** Cumulative isotopic data characterizing the DB-parallel nodules (black full dots) and bedding-parallel ones (empty dots) inside the Loiano Sandstones. **(b)** Isotopic data from the DB-related nodules (black full dots) and cement sampled in the calcrete (empty dots) in the Bollène quarry (see the Supplement S2 for details).

6 Cement stable isotope geochemistry

6.1 Loiano

Cement from the nodules of the Loiano samples has $\delta^{13}C$ values between -7.68 ‰ and -1.47 ‰ (VPDB) and $\delta^{18}O$ values between -4.42 ‰ and -1.35 ‰ (VPDB) (Fig. 12a). The cement from DB-related nodules is characterized by isotope compositions between -5.41 ‰ and -1.47 ‰ (VPDB) for $\delta^{13}C$ and between -4.42 ‰ and -1.40 ‰ for $\delta^{18}O$ (VPDB). The cement from bedding-parallel nodules has isotope compositions between -7.68 ‰ and -5.94 ‰ (VPDB) for $\delta^{13}C$ and between -2.09 ‰ and -1.35 ‰ (VPDB) for $\delta^{18}O$. Both cement groups (DB-parallel and bedding-parallel nodules) have a relatively narrow range of oxygen isotopic composition featuring a nearly vertical alignment in the $\delta^{18}O$–$\delta^{13}C$ cross-plot. DB-parallel nodules show a slightly wider span of $\delta^{18}O$ composition when compared to bedding-parallel nodules. However, carbon isotopic composition shows a wide range of variability when considering

both the total isotopic composition data and the cement group data.

6.2 Bollène

Stable isotope analysis of the Bollène samples also defines two groups of data in the δ^{18}O–δ^{13}C space (Fig. 12b). The cement group referring to the DB-related nodules has δ^{13}C values between −7.73 m and −4.68 ‰ (VPDB) and δ^{18}O values between −7.70 ‰ and −5.88 ‰ (VPDB). The other group is from cement sampled in a calcrete level observed within the same Turonian Sandstone a few meters above the studied outcrop (see Sect. 4.2 and the Supplement S2 for details), and it is characterized by isotope compositions between −2.54 ‰ and −2.39 ‰ (VPDB) for δ^{13}C and between −6.58 ‰ and −6.32 ‰ (VPDB) for δ^{18}O. Both cement groups have a relatively similar δ^{18}O signature and a relatively narrow range of δ^{18}O composition varying only between −7.70 ‰ and −5.88 ‰ (VPDB). In a similar way, cement sampled from the calcrete has a narrow range of δ^{13}C composition and shows heavier δ^{13}C values in the data set. However, the δ^{13}C composition of DB-related nodules has a wider variability range and is the most depleted in the data set.

7 Discussion

In the following, we compare the two field sites, highlighting their similarities and differences concerning the interaction between deformation, fluid flow, and diagenesis. We discuss the influence of DBs on fluid flow and their role in enhancing diagenesis and localizing diagenetic products (nodules). Finally, we propose an explanation for the geochemical environment within which fluids were sourced and precipitated the nodule cement. We then explore the implications of SDHs for subsurface fluid flow and reservoir characterization.

7.1 Cement distribution and its relationship with deformation bands

The distinctive feature of the Loiano Sandstones is a spatially heterogeneous cementation in the form of nodules. Field evidence indicates that DB formation predates calcite cementation. All nodules are spatially related to DBs (Figs. 3 and 5a–c) except for those that are situated along bedding planes (∼ 25 % of the total nodules; Figs. 3 and 5d, e). In contrast, not all DBs are associated with nodules. A clear correspondence always exists between the shape and elongation direction of the nodules and the DBs direction. This pattern is also observed from aerial photographs (Del Sole and Antonellini, 2019). Localized cement along these structural features is itself an indication that deformation preceded cement precipitation (e.g., Eichhubl et al., 2004). If the sandstones were completely cemented at first and then completely removed except from the DBs, the cement in the DB matrix would most likely have been preserved in orange–reddish hues (oxidation residues), but nothing like that was observed. Moreover, cement morphologies adjacent to the porosity at nodule edges imply that cement dissolution has not occurred (Fig. 10m, n), thus excluding the possibility that nodules, both those parallel to bedding and those parallel to DBs, are relicts from an overall dissolution process. No DBs crosscut the cement, at least for those sets that are spatially related to nodules (NNW–SSE to NE–SW), indicating that cementation postdates DB development. In support of this, the precipitation of cement and (the consequent) lower porosity would favor the formation of joints over DBs in the sandstone (Flodin et al., 2003; Aydin et al., 2006; Fig. 5a, b). The presence of pore-filling cement would increase the strength of the sandstone (Del Sole et al., 2020), preventing rotation and sliding of particles, and increase rock cohesion (Bernabé et al., 1992) and grain contact area, thus yielding a uniform contact stress distribution and higher stiffness (Dvorkin et al., 1991). Extensive cement, then, would inhibit DB development.

Results from microstructural observations show that intergranular cement in the nodules encloses the grains within both host rock and DBs, and it overprints burial-related mechanical and chemical compaction features (Fig. 10a–h). This evidence suggests that the formation of authigenic cements occurred after significant compaction (Cibin et al., 1993; Milliken et al., 1998). Estimated burial depths for the top of the Loiano Sandstones are 800–1000 m (Cibin et al., 1993) and 700–1200 m (McBride et al., 1995). Transgranular microfractures at grain contacts are due to stress concentration at contact points and they are interpreted as load-bearing structures within the granular framework (e.g., Antonellini et al., 1994; Eichhubl et al., 2010; Soliva et al., 2013). In DB-parallel nodule samples the cement that fills the transgranular fractures is in continuity (i.e., same textural and CL characteristics) with the pore-filling cement outside the fractures. The presence of undeformed cement within structural-related features such as microfractures and crushed grains (Fig. 10i–l), both within and outside the DBs, proves that cement precipitation occurred after (at least after the early stages of) deformation.

The bands are the main controlling factor on the location, geometry, and elongation direction of DB-parallel nodules. The occurrence and location of bedding-parallel nodules are instead controlled by grain size and contrast in grain size within the host rock. Although bedding-parallel nodules are found in all sands, they are more common within coarse-grained levels (≥ medium sands; i.e., size range: 0.25–0.5 mm). There are no nodules in sediments below the sand range or in layers with permeability below 100 mD (Del Sole et al., 2020). Moreover, bedding-parallel nodules are often restricted to the sand level in contact with clay–silty levels (Fig. 5d, e) above and/or below. Hence, grain size and permeability variations are the most important factors control-

ling diagenesis and nodule formation in Loiano. The grain size and permeability variations as dominant controls on nodule development in porous media is also reported by other authors (Mozley and Davis, 1996; Hall et al., 2004; Davis et al., 2006; Cavazza et al., 2009; Balsamo et al., 2012). In general, bedding-parallel nodules show a more rounded morphology when compared to DB-related nodules. The former nodule type owes its smooth morphology to a homogeneous and isotropic weathering; the sharp and squared shapes of DB-parallel nodules is probably due to the anisotropy introduced by the DBs in the host rock that influences the cementation. The interplay between band strength and erosion may also have an influence on nodule shape.

In the Bollène quarry, all calcite nodules occur in association with the DBs, in particular with the NW–SE/NNW–SSE set (Fig. 6b). At this site, we observe complex relationships among multiple deformational and diagenetic events. Timing of bands and nodules is inferred from crosscutting relationships. There is no evidence of low-angle ESE–WNW reverse-sense DBs crosscutting the cement nodules, whereas NE–SW- to ENE–WSW-trending strike-slip DBs offset the reverse-sense bands, the NW–SE bands, and the NW–SE-trending cement nodules (Figs. 6b and 7). The localization and parallelism between DBs and cement are similar at the two field sites, with the exception that NW–SE-trending nodules and DBs in Bollène are not superposed. Here, DBs are always overprinted by cement but the spatial overlap between DBs and nodules (Fig. 7e) is unusual. Nodules occur in compartments that are spatially confined by DB zones. Tabular nodules and clusters of spherical nodules are oriented with the major axis parallel to the NW–SE DBs (Figs. 6b and 7a). The NW–SE bands do not crosscut the cement; therefore, calcite cementation occurred between the NW–SE band formation (Pyrenean contraction or Oligocene–Miocene extension?) and the NE–SW strike-slip bands (Miocene–Quaternary age Alpine shortening?). Please refer to Supplement S1 for details on how DBs relate to the tectonics of the area. Microstructural observations show that the dominant phase of intergranular calcite cement encloses the grains within the nodules, and it overprints only a proportion of the transgranular microfractures at grain contact points. All microfractures in the nodules are filled by a cement that is in continuity (same texture and CL characteristics) with the pore-filling cement outside the grain. Unfilled microfractures (Fig. 11b) were not connected to the pore network, and they were potentially quickly isolated by the calcite mineral growing in the pore space. It is less likely that they formed after cement precipitation; otherwise, the cement would have been broken.

7.2 Role of deformation bands in fluid flow and diagenesis

The localized diagenesis observed in the form of nodules at Loiano and Bollène provides evidence for the effect of structural heterogeneities, such as DBs, on fluid flow in porous sandstones (Eichhubl et al., 2004, 2009; Balsamo et al., 2012; Philit et al., 2015; Del Sole and Antonellini, 2019; Pizzati et al., 2019; Del Sole et al., 2020). The petrophysical properties (porosity, permeability, capillary entry pressure) of DBs influence fluid flow and localize diagenesis and cement precipitation.

Cataclastic DBs increase flow tortuosity in reservoirs and produce capillary barriers that severely baffle the flow at the reservoir scale and limit cross-flow between host rock compartments (Harper and Mofta, 1985; Edwards et al., 1993; Lewis and Couples, 1993; Antonellini and Aydin, 1994; Leveille et al., 1997; Gibson, 1998; Antonellini et al., 1999, 2014; Sternlof et al., 2004; Rotevatn and Fossen, 2011; Ballas et al., 2012; Medici et al., 2019; Romano et al., 2020). Smaller pores within bands result in higher capillary forces than in the host rock. This may cause higher water saturation within the bands with respect to the host rock (Tueckmantel et al., 2012; Liu and Sun, 2020). A higher degree of flow tortuosity (reduction in pore interconnectivity) and lower porosity and permeability within the bands may increase the fluid retention time regardless of the water saturation conditions (Antonellini et al., 1999; Sigda and Wilson, 2003; Wilson et al., 2006). Recently, Romano et al. (2020) documented with single and multiphase core flooding experiments that cataclastic bands can strongly influence the fluid velocity field. Other authors (Taylor and Pollard, 2000; Eichhubl et al., 2004) recognized that a slower rate of solute transport relative to the fluid within the bands causes the formation and local perturbation of diagenetic alteration fronts. In light of these considerations and the temporal and spatial relationships between bands and cements obtained from field and microstructural observations, we discuss a model for selective cement precipitation associated with DBs. In our model we assume a reservoir in saturated conditions (see also Sect. 7.3).

A marked grain surface roughening and reduction of grain size, porosity, and pore size characterize the DBs presented in this work. In Loiano, the combined effect of cataclasis and compaction in the DBs causes porosity reduction by 1 order of magnitude, permeability reduction by 3 orders of magnitude, and advective velocity reduction by 2 orders of magnitude with respect to the host rock (Del Sole and Antonellini, 2019; Supplement S3). Similarly, DBs in the Bollène quarry have lower permeability (up to 3 orders of magnitude) and porosity (up to 50 %) (Ballas et al., 2014; see also Supplement S3) when compared to the host rock. A lower permeability, a higher degree of tortuosity (i.e., lower pore size), and reduced section area available for flow (i.e., lower porosity) in the DBs compared to the host rock may cause a flow "slowdown". In Loiano, the slowdown effect would be more pronounced when considering the normal-to-DB flow than the parallel-to-DB one given that normal-to-DB permeabilities are lower (1 order of magnitude in average) when compared to parallel-to-DB ones (Del Sole et al., 2020). Cata-

clasis has competing effects on advective flow velocity; it causes (i) an increase in flow velocity linked to the porosity reduction and (ii) a decrease in the hydraulic conductivity (if the hydraulic gradient does not change). The decrease in hydraulic conductivity (3 orders of magnitude; Del Sole and Antonellini, 2019) dominates over the flow velocity increase caused by porosity reduction (1 order of magnitude; Del Sole and Antonellini, 2019). As a result, there is a net decrease in advective flow velocity in the DBs. A reduction in flow velocity (i.e., slower flow path in the DB with respect to the host rock) might increase the residence time of the fluid migrating through the reactive material (see next paragraph).

A first mechanism responsible for cement nucleation in association with DBs would be the presence of highly reactive crushed and pervasive fractured siliciclastic grains within the cataclastic DBs (e.g., Lander et al., 2009; Williams et al., 2015). The comminuted material of the DBs has a large amount of reactive surface area (nucleation spots) and very tiny pore spaces among the crushed grains. With these conditions, cement precipitation requires less free energy to occur (Wollast, 1971; Berner, 1980), whereas greater cement abundances (e.g., Walderhaug, 2000) and faster rates of cement emplacement (Lander et al., 2008; Williams et al., 2015) are promoted. Despite the fact that the role of fracturing in promoting cement precipitation in sandstones has been essentially explored for quartz cement, we think that this mechanism can be applied to calcite cement too. There is plenty of evidence of calcite precipitation over a silica substrate (e.g., Stockmann et al., 2014), but it would require either more time or a higher degree of supersaturation (e.g., Noiriel et al., 2016) to occur (i.e., to lower the energy barrier for nucleation) when compared to a carbonate substratum. This mechanism has already been proposed to explain the presence of (quartz and calcite) cement within the band pore space and contrast in the degree of cementation between the bands and the surrounding rock (Antonellini et al., 1994; Knipe et al., 1997; Fisher and Knipe, 1998; Milliken et al., 2005; Philit et al., 2015; Del Sole and Antonellini, 2019; Pizzati et al., 2019). In this work we show that DBs are a preferred site of cement precipitation. Within the DB there are more nucleation spots for cement nucleation and smaller pores that lead to fast pore clogging. DB pores close faster than host rock ones. Once the cement begins to precipitate, the fresh carbonate substrate (cement) could further enhance precipitation (e.g., Noiriel et al., 2016). This mechanism may be relevant for Loiano where the calcite cement fills small pore spaces among fresh quartz and feldspar surfaces created during fracturing. This process can explain why in most cases DBs are more cemented than the surrounding host rock. On the contrary, this process was less relevant in the Bollène quarry where the bands are not cemented by carbonate and the cementation is localized in compartments between zones of bands rather than within them. The arrangement of nodules in Bollène indicates that the low-permeability DBs hindered the cross-flow, restricted the fluid flow, and focused the diagenesis to parallel-to-bands compartments.

A second mechanism could have worked in combination with the presence of more reactive fine-grained comminution products to promote cementation in the DBs in Loiano. According to their experiments on an analog fault gouge, Whitworth et al. (1999) suggested a membrane behavior for faults in sandstone during cross-fault flow and solute-sieving-aided calcite precipitation. A membrane effect and solute sieving by faults may locally increase the concentrations of components needed for calcite cementation (e.g.. Ca and bicarbonate) on the high-pressure side of the membrane and induce precipitation. The DBs could have acted as a semipermeable membrane in baffling chemically reactive flow and favor cement precipitation. This process may explain a higher concentration of cement along the DBs in nodules and the asymmetric distribution of cement on one side of DBs (upstream side; Figs. 4c, e and 9a, e). An analogous mechanism was proposed by other authors to explain the occurrence of the preferred and asymmetric distribution of the authigenic alterations (carbonate and clay cements, Eichhubl, 2001; hematite bleaching, Eichhubl et al., 2004) on the upstream side of DBs in sandstones.

Other factors that may have locally favored (the initiation of) calcite cement precipitation are the growth of cement on detrital grains (Loiano, Fig. 10e; Bollène, Fig. 11c) and the presence of broken detrital carbonate clasts (e.g., shell fragments) that act as a "seed" (cement nucleation sites) (e.g., Bjørkum and Walderhaug, 1990). The latter case was observed in Loiano, mainly in bedding-parallel nodules (Fig. 9c, d). The mechanisms discussed above explain how and why cement precipitation would occur within the band and in its proximity, as observed on-site. Our field observations confirm the theoretical and flow simulations as well as the analog experiments, which demonstrated that DBs can negatively affect the fluid flow in porous sandstones (e.g., Rotevatn and Fossen, 2011; Antonellini et al., 2014; Romano et al., 2020) and enhance cement precipitation (e.g., Lander et al., 2009; Williams et al., 2015).

7.3 Structural diagenesis scenario for carbonate nodule formation

We integrate petrographic observations and the stable isotope characterization of cements here with the mesoscale spatial organization and microscale textural relationships between nodules and DBs to discuss the geochemical conditions and potential fluid sources that controlled the formation of carbonate nodules in the studied areas. In Loiano, the first calcite cement to precipitate was the intraskeletal and pore-lining cement associated with bioclasts in bedding-parallel nodules (Fig. 9c–d). The cement fabric and textures, circumgranular dogtooth and void-filling drusy mosaic, suggest a phreatic environment (Longman, 1980; Moore, 1989; Adams and Diamond, 2017). Drusy calcite spars can result from re-

placement of aragonite in bioclasts in meteoric environments (Flügel, 2013). The second, more pervasive phase of cementation is documented by the intragranular cement observed in all the nodules. The mosaic of blocky sparite with coarse crystals and homogeneous distribution also point to phreatic conditions (Longman, 1980; Flügel, 2013; Adams and Diamond, 2017). The intergranular cement pattern is analogous in DB-parallel nodules and bedding-parallel nodules, meaning they probably formed in a similar phreatic environment.

Oxygen isotope data suggest a meteoric environment (Fig. 12a). According to the compilation made by Nelson and Smith (1996), the moderately depleted $\delta^{18}O$ and $\delta^{13}C$ values we found in both types of nodules (Fig. 12a) are grouped in the field of "meteoric cements" (Nelson and Smith, 1996) and are in support of precipitation under meteoric conditions. The $\delta^{18}O$ values of DB-parallel nodule cement correspond to parent fluids with an oxygen isotope composition ($\delta^{18}O_{fluid}$) varying from $-5.42‰$ to $-2.31‰$ Vienna Standard Mean Ocean Water (VSMOW) (precipitation at 14 °C) or from $-4.01‰$ to $-0.90‰$ VSMOW (precipitation at 20 °C; see Supplement S4 for details on the back calculation of $\delta^{18}O$ of parent fluids). These values are slightly less depleted if compared with the expected $\delta^{18}O$ of present-day meteoric fluids characterizing this area ($-8/-6‰$; Giustini et al., 2016). The isotopic signal of the cementing fluids may have been buffered by interaction with the host rock (dissolution of detrital marine shells in the sandstone framework; e.g., Fig. 10c–d), by mixing with local formation water (McBride et al., 1995), or, for instance, by more regional factors (e.g., atmospheric temperature, humidity, precipitation, seasonality of precipitation and recharge, vegetation; Cortecci et al., 2008; Jasechko, 2019). In this view, further investigations would be needed to properly constrain the cementing fluid conditions (e.g., clumped isotopes, fluid inclusions). The $\delta^{13}C$ composition of cement (Fig. 12a), however, seems to reflect soil weathering processes as the primary source of bicarbonate dissolved in the waters (Hudson, 1977; Nelson and Smith, 1996) and supports precipitation from meteoric fluids. DB-parallel and bedding-parallel nodules show a similar composition for $\delta^{18}O$; however, bedding-parallel nodules have more depleted $\delta^{13}C$ values. This might reflect a higher contribution of organic carbon from soil-derived CO_2 (Hudson, 1977), possibly indicating that bedding-parallel nodules formed in shallower conditions with respect to DB-parallel nodules. Another explanation is that the two types of nodules were formed by different episodes of water inflow with different (external) environmental conditions. The difference in isotopic composition between these two types of nodules indeed suggests different cement precipitation timing and water compositions as proposed by McBride et al. (1995) and Milliken et al. (1998). Phreatic meteoric conditions for nodule formation point to a shallow diagenesis, and it is consistent with the shallow burial depths estimated for the Loiano Sandstones (see Sect. 7.1).

Cementation patterns can be used to infer the paleo-fluid flow direction at the time of calcite precipitation (Mozley and Goodwin, 1995; Mozley and Davis, 1996; Cavazza et al., 2009; Eichhubl et al., 2009; Balsamo et al., 2012). The different spatial arrangements between DBs and nodules in Loiano make the paleo-fluid flow direction reconstruction challenging. The asymmetric distribution of cement in some nodules associated with DBs can be explained by lateral fluid circulation (Fig. 13a), and cement would accumulate on the upstream side of the DBs (Figs. 4c, 9, and 13a). In other cases, cement is roughly symmetrical with respect to the bands, or it is placed where conjugate bands intersect (Figs. 4b, 5c, and 13a). The most likely interpretation is that both lateral flow under saturated conditions and "direct" meteoric infiltration from the surface, with percolation through the rock, contributed to the formation of nodules in Loiano (Fig. 13a).

Calcite (i.e., diffusive supply of Ca^{2+} and HCO^{3-}) is possibly derived from the infiltration of $CaCO_3$-saturated meteoric fluids carrying soil-derived CO_2 (Hudson, 1977; Nelson and Smith, 1996), and/or it is locally derived from detrital carbonate grains in the sandstone layers or from intra-formational shale beds and calcite-rich clays layers (McBride et al., 1995; Milliken et al., 1998). In both scenarios calcite precipitates in correspondence to zones of DBs (DB-parallel nodules) and close to low-conductivity layers (bedding-parallel nodules). McBride et al. (1995) suggest that calcite precipitation along faults (DBs) in Loiano was induced by the mixing of locally derived formation water with meteoric water introduced along the faults or, alternatively, by a loss (exsolution) of CO_2 along the fault zones. These mechanisms, however, imply that DBs were fluid conductive. This hypothesis is at odds with our measurements of the DB hydraulic behavior (Del Sole and Antonellini, 2019; Del Sole et al., 2020). More likely, carbonate DB cementation resulted from CO_2-saturated groundwater (Fig. 13a). We cannot exclude the possibility of a role played by normal faults in the area (Picotti and Pazzaglia, 2008; Picotti et al., 2009; Fig. 2a) that might have steered regional subsurface fluid circulation. These faults could have cut through top and/or bottom seals and driven fluid migration from above and/or underneath aquifers (Fig. 13a). Episodic fault activity can also favor (episodic) horizontal fluid migration along layering at the time of faulting, possibly explaining the occurrence of nodules (Fig. 13a) and their different isotopic signature (Fig. 12a). From our observations, we can say that the selective cementation process in the Loiano Sandstones depends on "regional" hydrological factors (e.g., topographic gradient, bedding, faults?) locally coupled to the presence of DBs.

In the Bollène quarry, the relative timing of DB formation and cementation in the Turonian Sandstones is complex to unravel. Carbonate cementation occurred between distinct deformation phases with multiple DBs forming (see Sect. 7.1). The dominant dark cathodoluminescence pattern and homogeneously distributed poikilotopic spar texture

could suggest an oxidizing (high pO_2) meteoric phreatic environment (Longman, 1980; Moore, 1989; Flügel, 2013; Hiatt and Pufhal, 2014). Oxygen isotope data also support a meteoric source for the fluids (Fig. 12a). The range of moderately depleted $\delta^{18}O$ and $\delta^{13}C$ values of nodules in Bollène is consistent with a meteoric environment in a continental setting (Nelson and Smith, 1996). The $\delta^{18}O$ values of nodule cement correspond to parent fluids with an oxygen isotope composition ($\delta^{18}O_{fluid}$) varying between -7.85 ‰ and -5.98 ‰ VSMOW (see Supplement S4 for details on the back calculation of $\delta^{18}O$ of parent fluids). These values are consistent with the expected $\delta^{18}O$ of present-day meteoric fluids characterizing this area (e.g., Genty et al., 2014; Jasechko, 2019), thus supporting precipitation from meteoric fluids. Maximum burial depth of the Turonian Sandstone was estimated through stratigraphic constraints to be 400 ± 100 m (Ballas et al., 2013; Soliva et al., 2013). These data support the shallow conditions for nodule diagenesis in Bollène. A phreatic environment is more probable given that in vadose conditions we should have observed meniscus cements and because massive calcrete such as observed in the study area generally forms in a groundwater environment (e.g., Alonso-Zarza, 2003). The $\delta^{18}O$ values of cement from the calcrete layer correspond to parent solutions with $\delta^{18}O$ varying from -6.70 ‰ to -6.44 ‰ VSMOW (see Supplement S4), suggesting a meteoric source of fluids. In the vadose zone, DBs would also enhance unsaturated flow relative to the host rock (Sigda et al., 1999; Wilson et al., 2006; Cavailhes et al., 2009; Balsamo et al., 2012).

Field evidence suggests that clusters of low-permeability DBs in Bollène impeded cross-fault flow since no cement was found in superposition with the DBs. The presence of nodules between the DB clusters indicates that the DBs forced the fluid flow and localized the diagenesis in parallel-to-band compartments. This evidence and the fact that nodules are homogenous along their elongation direction discredit the hypothesis of lateral flow. The cement could have been originated from (i) downward fluid flow directly from infiltration of meteoric waters or (ii) upward flow of basinal fluid (pressurized aquifer) along fractures and fault pathways in the carbonate rocks (Fig. 13b). In both cases, the water flow was potentially driven by the vertical continuity of DB clusters that have acted as propagation features of faults in overlying (i) or underlying (ii) series and aquifers (Fig. 13b). This scenario might explain why the cement is found only in association with the NW–SE DBs. In both cases (i and ii), the constituent necessary for the precipitation of cement in nodules (i.e., Ca and bicarbonate) would come from the surrounding carbonates. Above the Turonian Sandstones there are several carbonate layers in the upper Turonian and Santonian interval (Fig. 2c; Ferry, 1997), whereas below there are carbonates belonging to the Jurassic and Cretaceous series (Fig. 2b, c; Debrand-Passard et al., 1984). In the first case (i), continental meteoric waters saturated with meteoric carbon dioxide have dissolved the necessary constituents along their path through the rock succession toward the high-porosity Turonian Sandstones. The water percolation through the soil favored fluid acidification. Similar depleted $\delta^{18}O$ values between nodules and cement from the calcrete level (Fig. 12b) support the (i) hypothesis, and they may have originated from a similar surficial cement source from downward water flow in association with variations of bicarbonate concentration and/or pH in the water table. In the second (ii) hypothesis, nodule cement resulted from CO_2 exsolution during the upward flow of basinal brine or CO_2-saturated groundwater in a pressurized aquifer.

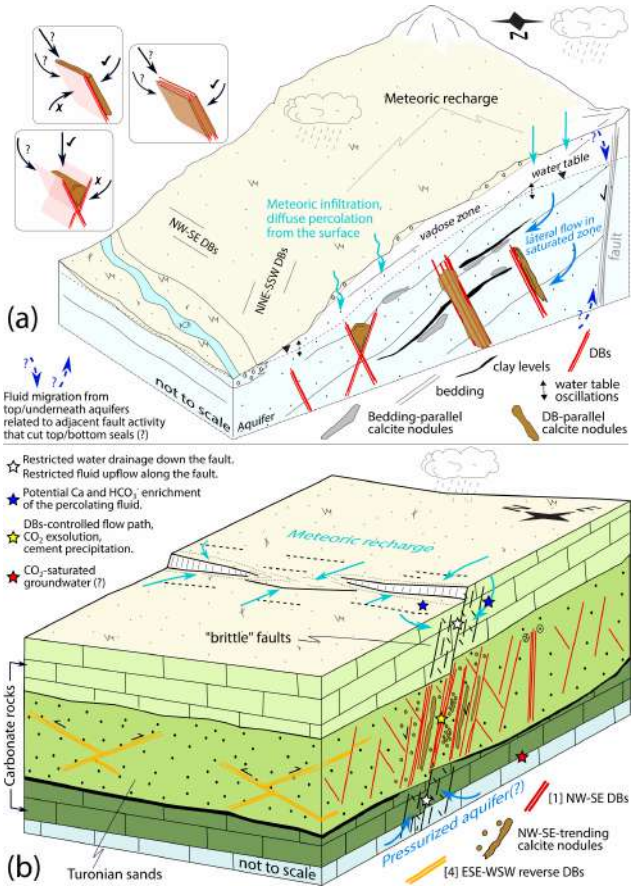

Figure 13. Generalized conceptual model for calcite nodule precipitation in the two study areas: **(a)** Loiano and **(b)** Bollène. See text (Sect. 7.3) for details. The inset sketches in **(a)** show a possible paleo-fluid flow direction at the time of calcite precipitation for different DB–nodule configurations.

7.4 Implications for subsurface fluid flow, reservoir characterization, and resource development

Models for calcite cementation are of fundamental importance for predicting sandstone and fault-rock properties such as porosity, permeability, compressibility, and seismic attributes. In Loiano, DBs have acted as fluid flow baffles. First, they buffered the fluid flow and localized cement precipita-

tion, acting as areas of preferential cementation in otherwise excellent-porosity sandstones. The resulting diagenetic products enhance porosity and permeability reduction caused by cataclasis, further affecting subsequent fluid circulation. The presence of structural-related cement in the form of concretions (i) strengthens the rock volume, (ii) degrades porosity and permeability, thereby increasing the buffering effect or sealing capacity of DBs, and (iii) imparts mechanical and petrophysical anisotropy to the host rock (Del Sole et al., 2020). We think that it is important to consider the possibility of concretions to form in association with faults within siliciclastic reservoirs, especially where these structures (DBs) are below seismic resolution (e.g., Del Sole et al., 2020). It is also critical to understand SDH spatial organization, extension, continuity, density, hydraulic role in terms of fluid flow circulation, and mechanical influence on the host rock. This information should be included in a robust reservoir characterization, and, in general, it is beneficial during geofluid exploration and energy appraisal, resource development strategies (groundwater, geothermal, hydrocarbon), well production, reservoir simulation modeling, geomechanical evaluation of a drilling site, and other environmental and industrial operations (e.g., waste fluid disposal; groundwater contaminants; geologic CO_2 sequestration; enhanced oil recovery – EOR). The incorporation of this information into aquifer or reservoir (flow) models requires implicit representation of the SDH network and the upscaling of its structural and petrophysical properties (e.g., Fachri et al., 2013; Antonellini et al., 2014). When the cementation is heterogeneous, such as in the examples presented in our work, it could be difficult to model and predict, especially when data are spatially discontinuous (e.g., wells). In these cases, outcrop-based studies allow for continuous and more reliable reconstructions of cement distribution. The characterization of the SDH network distribution (e.g., Del Sole et al., 2020) allows us to predict where (i.e., location and volumes) and how (i.e., spatial organization) the reservoir compartments are arranged and how the fluid circulation can be affected. The kind of study that we present here might be helpful to extract those statistical parameters necessary to implement reservoir studies that account for heterogeneity in petrophysical properties and their association with seismic and sub-seismic structural heterogeneities.

8 Conclusions

In this contribution, we present two examples of structural control exerted by DBs on fluid flow and diagenesis recorded by calcite nodules strictly associated with DBs. The objective of this research was to constrain the role of DBs in affecting the flow pattern and in localizing cement precipitation in porous sandstones, as well as to elucidate the mechanisms involved in these processes. The major results of our study can be summarized as follows.

1. At both study sites, one or more sets of DBs precede and control selective calcite cement precipitation in the form of nodules. The later localization of cementation along these structural features results in a complex and spatially heterogenous cementation pattern (SDHs).

2. Selective cementation of nodules associated with DBs indicates interaction between deformation structures, fluid flow, and chemical processes. The volumetrically significant presence of cement (10 %–25 % of the exposed outcrop volume) indicates that fluid flow and mass transport have been strongly affected by the presence of low-permeability DBs.

3. Two main processes are discussed to explain selective carbonate cementation associated with DBs in Loiano. (i) The high concentration of nucleation sites on fine-grained comminution products with increased reactive surface area of the pore–grain interface and small pore throats in the DB trigger cement precipitation and fast pore clogging with respect to the host rock. (ii) Solute sieving across the DB (membrane effect) promotes Ca and bicarbonate concentration increase on the upstream side.

4. In Bollène no clear superposition among bands and cement was observed. Here, the clusters of bands acted as hydraulic barriers to cross-flow, thus compartmentalizing fluid circulation and localizing diagenesis in volumes arranged parallel to the bands.

5. In both areas, cement textures, cathodoluminescence patterns, and their isotopic signature suggest that the cement in the nodules precipitated in a phreatic environment from fluids of meteoric origin.

6. In a framework of late-stage diagenesis (post-DB formation) and saturated conditions (phreatic environment), the processes commonly employed to explain focused fluid flow and preferential cement precipitation associated with DBs, such as "transient dilation" and "capillary suction" (see Sect. 1), appear not to be pertinent. In Bollène and Loiano the DBs buffered and compartmentalized fluid flow and localized diagenesis.

7. Further analyses, such as flow simulations and cement precipitation modeling, are deemed necessary to further explore microscale fluid flow and diagenetic mechanisms that drove preferential calcite cement precipitation along DBs in the studied porous sandstones.

8. DBs control flow pattern and affect how diagenetic heterogeneities are distributed within a porous sandstone. The association of diagenetic cementation with DBs further increases the flow-buffering potential of these structural features. It also creates SDHs that impart a mechanical and petrophysical anisotropy to the host

rock volume and can seriously affect the subsurface fluid circulation in porous sandstones. These features should be considered during reservoir characterization, especially where SDHs are below seismic resolution.

Data availability. All the data produced and used to write the paper are contained in it and in the Supplement. More detailed information will be made available on request by contacting the corresponding author.

Supplement. The supplement related to this article is available online at: https://doi.org/10.5194/se-11-2169-2020-supplement.

Author contributions. MA and LDS conceived the paper. LDS collected and processed field and laboratory data, provided their interpretations, drew the figures, wrote the paper, and did the revisions. RS and GB contributed to fieldwork at the Bollène study site and to cathodoluminescence data interpretation. MA, FB, and GV participated in fieldwork at the Loiano study site. All authors actively participated in discussing the results and drawing the conclusions, as well as critically revising the paper.

Competing interests. The authors declare that they have no conflict of interest.

Special issue statement. This article is part of the special issue "Faults, fractures, and fluid flow in the shallow crust". It is not associated with a conference.

Acknowledgements. Leonardo Del Sole kindly acknowledges Natalia A. Vergara Sassarini for fruitful discussion concerning the interpretation of cathodoluminescence imaging data and Mattia Pizzati for technical support during sampling for stable isotope analysis. The Laboratoire Géosciences Montpellier is acknowledged for hosting Leonardo Del Sole as a visiting PhD student in the period between April and July 2019, during which the cathodoluminescence analysis and the fieldwork in the Bollène quarry were carried out. The authors also wish to thank Paola Iacumin, Enricomaria Selmo, and Antonietta Di Matteo for stable isotope analysis in the SCVSA Department (University of Parma). Constructive criticism and comments by James P. Evans and Geoffrey C. Rawling greatly improved our paper. This research is part of a PhD project of the first author.

Leonardo Del Sole dedicates this work to the loving memory of Antonio Del Sole.

Review statement. This paper was edited by Randolph Williams and reviewed by Geoff Rawling and James Evans.

References

Adams, A. and Diamond, L. W.: Early diagenesis driven by widespread meteoric infiltration of a Central European carbonate ramp: A reinterpretation of the Upper Muschelkalk, Sediment. Geol., 362, 37–52, https://doi.org/10.1016/j.sedgeo.2017.10.002, 2017.

Alonso-Zarza, A. M.: Palaeoenvironmental significance of palustrine carbonates and calcretes in the geological record, Earth Sci. Rev., 60, 261–298, https://doi.org/10.1016/S0012-8252(02)00106-X, 2003.

Antonellini, M. and Aydin, A.: Effect of faulting on fluid flow in porous sandstones: petrophysical properties, AAPG Bull., 78, 355–377, https://doi.org/10.1306/BDFF90AA-1718-11D7-8645000102C1865D, 1994.

Antonellini, M., Aydin, A., and Pollard, D. D.: Microstructure of deformation bands in porous sandstones at Arches National Park, Utah, J. Struct. Geol., 16, 941–959, https://doi.org/10.1016/0191-8141(94)90077-9, 1994.

Antonellini, M., Aydin, A., and Orr, L.: Outcrop-aided characterization of a faulted hydrocarbon reservoir: Arroyo Grande oil field, California, USA, in: Faults and Subsurface Fluid Flow in the Shallow Crust, edited by: Haneberg, W. C., Mozley, P. S., Moore, J. C., and Goodwin, L. B., American Geophysical Union, Washington, DC, 113, 7–26, https://doi.org/10.1029/GM113p0007, 1999.

Antonellini, M., Cilona, A., Tondi, E., Zambrano, M., and Agosta, F.: Fluid flow numerical experiments of faulted porous carbonates, northwest Sicily (Italy), Mar. Pet. Geol., 55, 186–201, https://doi.org/10.1016/j.marpetgeo.2013.12.003, 2014.

Antonellini, M., Mollema, P. N., and Del Sole, L.: Application of analytical diffusion models to outcrop observations: implications for mass transport by fluid flow through fractures, Water Resour. Res., 53, 5545–5566, https://doi.org/10.1002/2016WR019864, 2017.

Antonellini, M., Del Sole, L., and Mollema, P. N.: Chert nodules in pelagic limestones as paleo-stress indicators: a 3D geomechanical analysis, J. Struct. Geol, 132, 103979, https://doi.org/10.1016/j.jsg.2020.103979, 2020.

Arthaud, F. and Seìguret, M.: Les structures pyreìneìennes du Languedoc et du Golfe du Lion (Sud de la France), Bull. Soc. Geìol. Fr., 23, 51–63, 1981.

Aydin, A.: Small faults formed as deformation bands in sandstones, Pure Appl. Geophys., 116, 913–930, 1978.

Aydin, A.: Fractures, faults, and hydrocarbon entrapment, migration and flow, Mar. Pet. Geol., 17, 797–814, https://doi.org/10.1016/S0264-8172(00)00020-9, 2000.

Aydin, A., Borja, R. I., and Eichhubl, P.: Geological and mathematical framework for failure modes in granular rock, J. Struct. Geol., 28, 83–98, https://doi.org/10.1016/j.jsg.2005.07.008, 2006.

Ballas, G., Soliva, R., Sizun, J. P., Benedicto, A., Cavailhes, T., and Raynaud, S.: The importance of the degree of cataclasis in shear bands for fluid flow in porous sand- stone, Provence, France, AAPG Bull., 96, 2167–2186, https://doi.org/10.1306/04051211097, 2012.

Ballas, G., Soliva, R., Sizun, J. P., Fossen, H., Benedicto, A., and Skurtveit, E.: Shear-enhanced compaction bands formed at shallow burial conditions; implications for fluid flow (Provence, France), J. Struct. Geol., 47, 3–15, https://doi.org/10.1016/j.jsg.2012.11.008, 2013.

Ballas, G., Soliva, R., Benedicto, A., and Sizun, J. P.: Control of tectonic setting and large-scale faults on the basin-scale distribution of deformation bands in porous sandstone (Provence, France), Mar. Pet. Geol., 55, 142–159, https://doi.org/10.1016/j.marpetgeo.2013.12.020, 2014.

Ballas, G., Fossen, H., and Soliva, R.: Factors controlling permeability of cataclastic deformation bands and faults in porous sandstone reservoirs, J. Struct. Geol., 76, 1–21, https://doi.org/10.1016/j.jsg.2015.03.013, 2015.

Balsamo F. and Storti F.: Grain size and permeability evolution of soft-sediment extensional sub-seismic and seismic fault zones in high-porosity sediments from the Crotone basin, southern Apennines, Italy, Mar. Pet. Geol., 27, 822–837, https://doi.org/10.1016/j.marpetgeo.2009.10.016, 2010.

Balsamo, F., Storti, F., and Gröcke, D. R.: Fault-related fluid flow history in shallow marine sediments from carbonate concretions, Crotone basin, south Italy, J. Geol. Soc., 169, 613–626, https://doi.org/10.1144/0016-76492011-109, 2012.

Barnaby, R. J. and Rimstidt, J. D.: Redox conditions of calcite cementation interpreted from Mn and Fe contents of authigenic calcites, Geol. Soc. Am. Bull., 101, 795–804, https://doi.org/10.1130/0016-7606(1989)101<0795:RCOCCI>2.3.CO;2, 1989.

Bense, V. F., Gleeson, T., Loveless, S. E., Bour, O., and Scibek, J.: Fault zone hydrogeology, Earth Sci. Rev., 127, 171–192, https://doi.org/10.1016/j.earscirev.2013.09.008, 2013.

Bernabé, Y., Fryer, D. T., and Hayes, J. A.: The effect of cement on the strength of granular rocks, Geophys. Res. Lett., 19, 1511–1514, https://doi.org/10.1029/92GL01288, 1992.

Berner, R. A.: Early Diagenesis: a Theoretical Approach, Princeton University Press, Princeton, NJ, 1980.

Bjørkum, P. A., and Walderhaug, O.: Geometrical arrangement of calcite cementation within shallow marine sandstones, Earth Sci. Rev., 29, 145–161, https://doi.org/10.1016/0012-8252(90)90033-R, 1990.

Boutt, D. F., Plourde, K. E., Cook, J., and Goodwin, L. B.: Cementation and the hydromechanical behavior of siliciclastic aquifers and reservoirs, Geofluids, 14, 189–199, https://doi.org/10.1111/gfl.12062, 2014.

Busch, B., Hilgers, C., Gronen, L., and Adelmann, D.: Cementation and structural diagenesis of fluvio-aeolian Rotliegend sandstones, northern England, J. Geol. Soc. London, 174, 855–868, https://doi.org/10.1144/jgs2016-122, 2017.

Cavailhes, T., Soliva, R., Benedicto, A., Loggia, D., Schultz, R. A., and Wibberley, C. A. J.: Are cataclastic shear bands fluid barriers or capillarity conduits? Insight from the analysis of redox fronts in porous sandstones from Provence, France, in: 2nd EAGE International Conference on Fault and Top Seals: From Pore to Basin Scale, Montpellier, France, 21–24 September 2009, 3 pp., https://doi.org/10.3997/2214-4609.20147185, 2009.

Cavazza, W., Braga, R., Reinhardt, E. G., and Zanotti, C.: Influence of host-rock texture on the morphology of carbonate concretions in a meteoric diagenetic environment, J. Sediment. Res., 79, 377–388, https://doi.org/10.2110/jsr.2009.047, 2009.

Champion, C., Choukroune, P., and Clauzon, G.: La deìformation post-mioceÌne en Provence occidentale, Geodinam. Act., 13, 67–85, https://doi.org/10.1080/09853111.2000.11105365, 2000.

Cibin, U., Cavazza, W., Fontana, D., Milliken, K. L., and McBride, E. F.: Comparison of composition and texture of calcite-cemented concretions and host sandstones, Northern Apennines, Italy, J. Sediment. Res., 63, 945–954, https://doi.org/10.1306/D4267C4E-2B26-11D7-8648000102C1865D, 1993.

Cortecci, G., Dinelli, E., and Mussi, M.: Isotopic composition and secondary evaporation effects on precipitation from the urban centre of Bologna, Italy, Period. Miner., 77, 55–63, https://doi.org/10.2451/2008PM0004, 2008.

Davis, J. M., Roy, N. D., Mozley, P. S., and Hall, J. S.: The effect of carbonate cementation on permeability heterogeneity in fluvial aquifers: An outcrop analog study, Sediment. Geol., 184, 267–280, https://doi.org/10.1016/j.sedgeo.2005.11.005, 2006.

Debrand-Passard, S., Courbouleix, S., and Lienhardt, M. J.: SyntheÌse geìologique du Sud- Est de la France: stratigraphie et paleìogeìographie, Bureau de Recherches Geìologiques et MinieÌres, Meìmoire, vol. 215 (Orleìans), 1984.

Del Sole, L. and Antonellini, M.: Microstructural, petrophysical, and mechanical properties of compactive shear bands associated to calcite cement concretions in arkose sandstone, J. Struct. Geol., 126, 51–68, https://doi.org/10.1016/j.jsg.2019.05.007, 2019.

Del Sole, L., Antonellini, M., and Calafato, A.: Characterization of sub-seismic resolution structural diagenetic heterogeneities in porous sandstones: Combining ground-penetrating radar profiles with geomechanical and petrophysical in situ measurements (Northern Apennines, Italy), Mar. Pet. Geol., 117, 104375, https://doi.org/10.1016/j.marpetgeo.2020.104375, 2020.

Dewhurst, D. N. and Jones, R. M.: Influence of physical and diagenetic processes on fault geomechanics and reactivation, J. Geochem. Exp., 78, 153–157, https://doi.org/10.1016/S0375-6742(03)00124-9, 2003.

Dvorkin, J., Mavko, G., and Nur, A.: The effect of cementation on the elastic properties of granular material, Mech. Mater., 12, 207–217, https://doi.org/10.1016/0167-6636(91)90018-U, 1991.

Edwards, H. E., Becker, A. D., and Howell, J. A.: Compartmentalization of an aeolian sandstone by structural heterogeneities: permo-Triassic Hopeman Sandstone, Moray Firth, Scotland, Geol. Soc. Spec. Publ., 73, 339–365, https://doi.org/10.1144/GSL.SP.1993.073.01.20, 1993.

Ehrenberg, S. N.: Relationship between diagenesis and reservoir quality in sandstones of the Garn formation, Haltenbanken, mid-Norwegian Continental shelf, AAPG Bull., 74, 1538–1558, https://doi.org/10.1306/0C9B2515-1710-11D7-8645000102C1865D, 1990.

Eichhubl, P.: Paleo-Fluid Flow Indicators, Stanford Rock Fracture Project, Vol. 12., 10 pp., available at: https://stacks.stanford.edu/file/druid:jp813ns8076/RFP_2001_Eichhubl.pdf (last access: 5 March 2020), 2001.

Eichhubl, P., Taylor, W. L., Pollard, D. D., and Aydin, A.: Paleo-fluid flow and deformation in the Aztec Sandstone at the Valley of Fire, Nevada – evidence for the coupling of hydrogeologic, diagenetic, and tectonic processes, Geol. Soc. Am., 116, 1120–1136, 2004.

Eichhubl, P., Davatzes, N. C., and Becker, S. P.: Structural and diagenetic control of fluid migration and cementation along the Moab fault, Utah, AAPG Bull., 93, 653–681, https://doi.org/10.1130/0016-7606(1974)85<1515:CATGOF>2.0.CO;2, 2009.

Eichhubl, P., Hooker, J. N., and Laubach, S. E.: Pure and shear-enhanced compaction bands in Aztec Sandstone, J. Struct. Geol., 32, 1873–1886, https://doi.org/10.1016/j.jsg.2010.02.004, 2010.

Fachri, M., Rotevatn, A., and Tveranger, J.: Fluid flow in relay zones revisited: Towards an improved representation of small-scale structural heterogeneities in flow models, Mar. Pet. Geol., 46, 144–164, https://doi.org/10.1016/j.marpetgeo.2013.05.016, 2013.

Faulkner, D. R., Jackson, C. A. L., Lunn, R. J., Schlische, R. W., Shipton, Z. K., Wibberley, C. A. J., and Withjack, M. O.: A review of recent developments concerning the structure, mechanics and fluid flow properties of fault zones, J. Struct. Geol., 32, 1557–1575, https://doi.org/10.1016/j.jsg.2010.06.009, 2010.

Ferry, S. (Ed.): Actes des Journeìes Scientifiques CNRS/ANDRA, Apport des forages ANDRA de Marcoule aÌ la connaissance de la marge creìtaceìe rhodanienne, Etude du Gard Rhodanien/EDP sciences, Bagnols-sur-CeÌze, 63–91, 1997.

Fisher, Q. J. and Knipe, R.: Fault sealing processes in siliciclastic sediments, Geol. Soc. Spec. Publ., 147, 117–134, https://doi.org/10.1144/GSL.SP.1998.147.01.08, 1998.

Flodin, E., Prasad, M., and Aydin, A.: Petrophysical constraints on deformation styles in Aztec Sandstone, southern Nevada, USA, Pure Appl. Geophys., 160, 1589–1610, https://doi.org/10.1007/s00024-003-2377-1, 2003.

Flügel, E.: Microfacies of carbonate rocks: analysis, interpretation and application, Springer Science & Business Media, 2013.

Fossen, H. and Bale, A.: Deformation and their influence on fluid flow, AAPG Bull., 91, 1685–1700, https://doi.org/10.1306/07300706146, 2007.

Fossen, H., Soliva, R., Ballas, G., Trzaskos, B., Cavalcante, C., and Schultz, R. A.: A review of deformation bands in reservoir sandstones: geometries, mechanisms and distribution, in: Subseismic-Scale Reservoir Deformation, edited by: Ashton, M., Dee, S. J., and Wennberg, O. P., Geol. Soc. Spec. Publ., 459, 9–33, https://doi.org/10.1144/SP459.4, 2017.

Fowles, J. and Burley, S.: Textural and permeability characteristics of faulted, high porosity sandstones, Mar. Pet. Geol., 11, 608–623, https://doi.org/10.1016/0264-8172(94)90071-X, 1994.

Genty, D., Labuhn, I., Hoffmann, G., Danis, P. A., Mestre, O., Bourges, F., Wainer, K., Massault, M., Van Exter, S., Reìgnier, E., Orengo, P., Falourd, S., and Minster, B.: Rainfall and cave water isotopic relationships in two South-France sites, Geochim. Cosmochim. Act., 131, 323–343, https://doi.org/10.1016/j.gca.2014.01.043, 2014.

Gibson, R. G.: Physical character and fluid-flow properties of sandstone-derived fault zones, Geol. Soc. Spec. Publ., 127, 83–97, https://doi.org/10.1144/GSL.SP.1998.127.01.07, 1998.

Giustini, F., Brilli, M., and Patera, A.: Mapping oxygen stable isotopes of precipitation in Italy, J. Hydrol., 8, 162–181, https://doi.org/10.1016/j.ejrh.2016.04.001, 2016.

Hall, J. S., Mozley, P., Davis, J. M., and Roy, N. D.: Environments of formation and controls on spatial distribution of calcite cementation in Plio-Pleistocene fluvial deposits, New Mexico, USA, J. Sediment. Res., 74, 643–653, https://doi.org/10.1306/020904740643, 2004.

Harper, T. and Moftah, I.: Skin effect and completion options in the Ras Budran Reservoir, in: Society of Petroleum Engineers Middle East Oil Technical Conference and Exhibition, 13708, 211–226, https://doi.org/10.2118/13708-MS, 1985.

Hiatt, E. E. and Pufahl, P. K.: Cathodoluminescence petrography of carbonate rocks: a review of applications for understanding diagenesis, reservoir quality and pore system evolution, Short Course, 45, 75–96, 2014.

Hudson, J. D.: Stable isotopes and limestone lithification, J. Geol. Soc. London, 133, 637–660, https://doi.org/10.1144/gsjgs.133.6.0637, 1977.

Jasechko, S.: Global isotope hydrogeology – Review, Rev. Geophys., 57, 835–965, https://doi.org/10.1029/2018RG000627, 2019.

Kantorowicz, J. D., Bryant, I. D., and Dawans, J. M.: Controls on the Geometry and Distribution of Carbonate Cements in Jurassic Sandstones: Bridport Sands, Southern England and Viking Group, Troll Field, Norway Geol. Soc. Spec. Publ., 36, 103–118, https://doi.org/10.1144/GSL.SP.1987.036.01.09, 1987.

Knipe, R. J., Fisher, Q. J., Jones, G., Clennell, M. R., Farmer, A. B., Harrison, A., Kidd, B., McAllister, E., Porter, J. R., and White, E. A.: Fault seal analysis: successful methodologies, application and future directions, Norwegian Petroleum Soc. Spec. Publ., 7, 15–38, https://doi.org/10.1016/S0928-8937(97)80004-5, 1997.

La Bruna, V., Lamarche, J., Agosta, F., Rustichelli, A., Giuffrida, A., Salardon, R., and Marié, L.: Structural diagenesis of shallow platform carbonates: Role of early embrittlement on fracture setting and distribution, case study of Monte Alpi (Southern Apennines, Italy), J. Struct. Geol., 131, 103940, https://doi.org/10.1016/j.jsg.2019.103940, 2020.

Labaume, P. and Moretti, I.: Diagenesis-dependence of cataclastic thrust fault zone sealing in sandstones. Example from the Bolivian Sub-Andean Zone, J. Struct. Geol., 23, 1659–1675, https://doi.org/10.1016/S0191-8141(01)00024-4, 2001.

Lander, R. H., Larese, R. E., and Bonnell, L. M.: Toward more accurate quartz cement models: The importance of euhedral versus noneuhedral growth rates, AAPG Bull., 92, 1537–1563, https://doi.org/10.1306/07160808037, 2008.

Lander, R. H., Solano-Acosta, W., Thomas, A. R., Reed, R. M., Kacewicz, M., Bonnell, L. M., and Hooker, J. N.: Simulation of fault sealing from quartz cementation within cataclastic deformation zones, in: AAPG Hedberg Conference Basinand Petroleum Systems Modeling: New Horizons in Research and Applications, Napa, California, USA, 3–7 May 2009.

Laubach, S. E., Olson, J. E., and Gross, M. R.: Mechanical and fracture stratigraphy, AAPG Bull., 93, 1413–1426, https://doi.org/10.1306/07270909094, 2009.

Laubach, S. E., Eichhubl, P., Hilgers, C., and Lander, R. H.: Structural diagenesis, J. Struct. Geol., 32, 1866–1872, https://doi.org/10.1016/j.jsg.2010.10.001, 2010.

Leveille, G. P., Knipe, R., More, C., Ellis, D., Dudley, G., Jones, G., Fisher, Q. J., and Allinson, G.: Compartmentalization of Rotliegendes gas reservoirs by sealing faults, Jupiter Fields area, southern North Sea, Geol. Soc. Spec. Publ., 123, 87–104, https://doi.org/10.1144/GSL.SP.1997.123.01.06, 1997.

Lewis, H. and Couples, G. D.: Production evidence for geological heterogeneities in the Anschutz Ranch East field, western U.S.A., in: Characterization of fluvial and eolian reservoirs, edited by: North, C. P. and Prosser, D. J., Geol. Soc. Spec. Publ., 73, 321–338, https://doi.org/10.1144/GSL.SP.1993.073.01.19, 1993.

Liu, Z. and Sun, Y.: Characteristics and formation process of contractional deformation bands in oil-bearing sandstones in the

hinge of a fold: A case study of the Youshashan anticline, western Qaidam Basin, China, J. Petrol. Sci. Eng., 189, 106994, https://doi.org/10.1016/j.petrol.2020.106994, 2020.

Lommatzsch, M., Exner, U., Gier, S., and Grasemann, B.: Structural and chemical controls of deformation bands on fluid flow: interplay between cataclasis and diagenetic alteration: structural and Chemical Controls of Deformation Bands on Fluid Flow, AAPG Bull., 99, 689–710, https://doi.org/10.1306/10081413162, 2015.

Longman, M. W.: Carbonate diagenetic textures from nearsurface diagenetic environments, AAPG Bull., 64, 461–487, https://doi.org/10.1306/2F918A63-16CE-11D7-8645000102C1865D, 1980.

Machel, H. G.: Application of cathodoluminescence to carbonate diagenesis, in: Cathodoluminescence in geosciences, edited by: Pagel, M., Barbin, V., Blanc, P., and Ohnenstetter D., Springer, Berlin, Heidelberg, 271–301, https://doi.org/10.1007/978-3-662-04086-7, 2000.

Main, I. G., Kwon, O., Ngwenya, B. T., and Elphick, S. C.: Fault sealing during deformation-band growth in porous sandstone, Geology, 28, 1131–1134, https://doi.org/10.1130/0091-7613(2000)28<1131:FSDDGI>2.0.CO;2, 2000.

Manzocchi, T., Ringrose, P. S., and Underhill, J. R.: Flow through fault systems in high-porosity sandstones, Geol. Soc. Spec. Publ., 127, 65–82, https://doi.org/10.1144/GSL.SP.1998.127.01.06, 1998.

Marroni, M., Meneghini, F., and Pandolfi, L.: A revised Subduction inception model to explain the late cretaceous, double-vergent orogen in the precollisional Western Tethys: Evidence from the Northern Apennines, Tectonics, 36, 2227–2249, https://doi.org/10.1002/2017TC004627, 2017.

Marshall, D. J.: Cathodoluminescence of geological Materials, Unwin Hyman, Boston, 1988.

McBride, E. F., Milliken, K. L., Cavazza, W., Cibin, U., Fontana, D., Picard, M. D., and Zuffa, G. G.: Heterogeneous distribution of calcite cement at the outcrop scale in tertiary sandstones, northern Apennines, Italy, AAPG Bull., 79, 1044–1063, https://doi.org/10.1306/8D2B21C3-171E-11D7-8645000102C1865D, 1995.

Medici, G., West, L. J., Mountney, N. P., and Welch, M.: Permeability of rock discontinuities and faults in the Triassic Sherwood Sandstone Group (UK): insights for management of fluvio-aeolian aquifers worldwide, Hydrogeology J., 27, 2835–2855, https://doi.org/10.1007/s10040-019-02035-7, 2019.

Milliken, K. L., McBride, E. F., Cavazza, W., Cibin, U., Fontana, D., Picard, M. D., and Zuffa, G. G.: Geochemical history of calcite precipitation in Tertiary sandstones, northern Apennines, Italy, in: Carbonate cementation in sandstones, edited by: Morad, S., International Association of Sedimentologists Special Publication 26, 213–239, https://doi.org/10.1002/9781444304893.ch10, 1998.

Milliken, K. L., Reed, R. M., and Laubach, S. E.: Quantifying compaction and cementation in deformation bands in porous sandstones, in: Faults, fluid flow, and petroleum traps, edited by: Sorkhabi, R. and Tsuji, Y., AAPG Mem., 85, 237–249, https://doi.org/10.1306/1033726M85252, 2005.

Moore, C. H.: Carbonate Diagenesis and Porosity, Elsevier, Amsterdam, 1989.

Morad, S., Al-Ramadan, K., Ketzer, J. M., and De Ros, L. F.: The impact of diagenesis on the heterogeneity of sandstone reservoirs: A review of the role of depositional facies and sequence stratigraphy, AAPG Bull., 94, 1267–1309, https://doi.org/10.1306/04211009178, 2010.

Mozley, P. S. and Davis, J. M.: Relationship between oriented calcite concretions and permeability correlation structure in an alluvial aquifer, Sierra Ladrones Formation, New Mexico, J. Sediment. Res., 66, 11–16, https://doi.org/10.1306/D4268293-2B26-11D7-8648000102C1865D, 1996.

Mozley, P. S. and Goodwin, L. B.: Patterns of cementation along a Cenozoic normal fault: a record of paleoflow orientations, Geology, 23, 539–542, https://doi.org/10.1130/B25618.1, 1995.

Nelson, C. S. and Smith, A. M.: Stable oxygen and carbon isotope compositional fields for skeletal and diagenetic components in New Zealand Cenozoic nontropical carbonate sediments and limestones: a synthesis and review, New Zeal. J. Geol. Geop., 39, 93–107, https://doi.org/10.1080/00288306.1996.9514697, 1996.

Noiriel, C., Steefel, C. I., Yang, L., and Bernard, D.: Effects of pore-scale precipitation on permeability and flow, Adv. Water Resour., 95, 125–137, https://doi.org/10.1016/j.advwatres.2015.11.013, 2016.

Ogilvie, S. R. and Glover, P. W.: The petrophysical properties of deformation bands in relation to their microstructure, Earth Planet. Sc. Lett., 193, 129–142, https://doi.org/10.1016/S0012-821X(01)00492-7, 2001.

Papani, L.: Le arenarie di Loiano nel contesto dell'Appennino settentrionale, PhD thesis, Universita di Bologna, Bologna, 40 pp., 1998.

Parnell, J., Watt, G. R., Middleton, D., Kelly, J., and Baron, M.: Deformation band control on hydrocarbon migration, J. Sediment. Res., 74, 552–560, https://doi.org/10.1306/121703740552, 2004.

Parry, W. T., Chan, M. A., and Beitler, B.: Chemical bleaching indicates episodes of fluid flow in deformation bands in sandstone, AAPG Bull., 88, 175–191, https://doi.org/10.1306/09090303034, 2004.

Pei, Y., Paton, D. A., Knipe, R. J., and Wu, K.: A review of fault sealing behaviour and its evaluation in siliciclastic rocks, Earth Sci. Rev., 150, 121–138, https://doi.org/10.1016/j.earscirev.2015.07.011, 2015.

Petrie, E. S., Petrie, R. A., and Evans, J. P.: Identification of reactivation and increased permeability associated with a fault damage zone using a multidisciplinary approach, J. Struct. Geol., 59, 37–49, https://doi.org/10.1016/j.jsg.2013.11.008, 2014.

Philit, S., Soliva, R., Labaume, P., Gout, C., and Wibberley, C.: Relations between shallow cataclastic faulting and cementation in porous sandstones: first insight from a groundwater environmental context, J. Struct. Geol., 81, 89–105, https://doi.org/10.1016/j.jsg.2015.10.001, 2015.

Philit, S., Soliva, R., Castilla, R., Ballas, G., and Taillefer, A.: Clusters of cataclastic deformation bands in porous sandstones, J. Struct. Geol., 114, 235–250, https://doi.org/10.1016/j.jsg.2018.04.013, 2018.

Philit, S., Soliva, R., Ballas, G., Chemenda, A., and Castilla, R.: Fault surface development and fault rock juxtaposition along deformation band clusters in porous sandstones series, AAPG Bull., 103, 2731–2756, https://doi.org/10.1306/01211917256, 2019.

Picotti, V. and Pazzaglia, F. J.: A new active tectonic model for the construction of the Northern Apennines mountain front

near Bologna (Italy), J. Geophys. Res.-Sol. Ea., 113, B08412, https://doi.org/10.1029/2007JB005307, 2008.

Picotti, V., Ponza, A., and Pazzaglia, F. J.: Topographic expression of active faults in the foothills of the Northern Apennines, Tectonophysics, 474, 285–294, https://doi.org/10.1016/j.tecto.2009.01.009, 2009.

Pizzati, M., Balsamo, F., Storti, F., and Iacumin, P.: Physical and chemical strain-hardening during faulting in poorly lithified sandstone: The role of kinematic stress field and selective cementation, Geol. Soc. Am. Bull., 132, 1183–1200, https://doi.org/10.1130/b35296.1, 2019.

Qu, D. and Tveranger, J.: Incorporation of deformation band fault damage zones in reservoir models, AAPG Bull., 100, 423–443, https://doi.org/10.1306/12111514166, 2016.

Romano, C. R., Zahasky, C., Garing, C., Minto, J. M., Benson, S. M., Shipton, Z. K., and Lunn, R. J.: Sub-core scale fluid flow behavior in a sandstone with cataclastic deformation bands, Water Resour. Res., 56, e2019WR026715, https://doi.org/10.1029/2019WR026715, 2020.

Rotevatn, A. and Fossen, H.: Simulating the effect of subseismic fault tails and process zones in a siliciclastic reservoir analogue: implications for aquifer support and trap definition, Mar. Pet. Geol., 28, 1648–1662, https://doi.org/10.1016/j.marpetgeo.2011.07.005, 2011.

Rotevatn, A., Sandve, T. H., Keilegavlen, E., Kolyukhin, D., and Fossen, H.: Deformation bands and their impact on fluid flow in sandstone reservoirs: the role of natural thickness variations, Geofluids, 13, 359–371, https://doi.org/10.1111/gfl.12030, 2013.

Roure, F., Brun, J. P., Colletta, B., and Van den Driessche, J.: Geometry and kinematics of extensional structures in the Alpine Foreland Basin of southeastern France, J. Struct. Geol., 14, 503–519, https://doi.org/10.1016/0191-8141(92)90153-N, 1992.

Saillet, E. and Wibberley, C. A. J.: Evolution of cataclastic faulting in high-porosity sandstone, Bassin du Sud-Est, Provence, France, J. Struct. Geol., 32, 1590–1608, https://doi.org/10.1016/j.jsg.2010.02.007, 2010.

Salvini, F.: Daisy 3: The Structural Data Integrated System Analyzer Software, University of Roma Tre, Rome, available at: http://host.uniroma3.it/progetti/fralab/Downloads/Programs/ (last access: 25 August 2020), 2004.

Sample, J. C., Woods, S., Bender, E., and Loveall, M.: Relationship between deformation bands and petroleum migration in an exhumed reservoir rock, Los Angeles Basin, California, USA, Geofluids, 6, 105–112, https://doi.org/10.1111/j.1468-8123.2005.00131.x, 2006.

Séranne, M., Benedicto, A., Labaume, P., Truffert, C., and Pascal, G.: Structural style and evolution of the gulf of Lion Oligo-miocene rifting: role of the Pyrenean orogeny, Mar. Pet. Geol., 12, 809–820, https://doi.org/10.1016/0264-8172(95)98849-Z, 1995.

Shipton, Z. K., Evans, J. P., Robeson, K. R., Forster, C. B., and Snelgrove, S.: Structural heterogeneity and permeability in faulted eolian sandstone: Implications for subsurface modeling of faults, AAPG bulletin, 86, 863–883, https://doi.org/10.1306/61EEDBC0-173E-11D7-8645000102C1865D, 2002.

Shipton, Z. K., Evans, J. P., and Thompson, L. B.: The geometry and thickness of deformation-band fault core and its influence on sealing characteristics of deformation-band fault zones, in: Faults, fluid flow, and petroleum traps, edited by: Sorkhabi, R. and Tsuji, Y., AAPG Mem., 85, 181–195, https://doi.org/10.1306/1033723M853135, 2005.

Sigda, J. M. and Wilson, J. L.: Are faults preferential flow paths through semiarid and arid vadose zones?, Water Resour. Res., 39, 1225, https://doi.org/10.1029/2002WR001406, 2003.

Sigda, J. M., Goodwin, L. B., Mozley, P. S., and Wilson, J. L.: Permeability alteration in small-displacement faults in poorly lithified sediments: Rio Grande Rift, Central New Mexico, in: Faults and Subsurface Fluid Flow in the Shallow Crust, edited by: Haneberg, W. C., Mozley, P. S., Moore, J. C., and Goodwin, L. B., American Geophysical Union, Washington, DC, 51–68, https://doi.org/10.1029/GM113p0051, 1999.

Soliva, R., Schultz, R. A., Ballas, G., Taboada, A., Wibberley, C., Saillet, E., and Benedicto, A.: A model of strain localization in porous sandstone as a function of tectonic setting, burial and material properties; new insight from Provence (southern France), J. Struct. Geol., 49, 50–63, https://doi.org/10.1016/j.jsg.2012.11.011, 2013.

Soliva, R., Ballas, G., Fossen, H., and Philit, S.: Tectonic regime controls clustering of deformation bands in porous sandstone, Geology, 44, 423–426, https://doi.org/10.1130/G37585.1, 2016.

Sternlof, K. R., Chapin, J. R., Pollard, D. D., and Durlofsky, L. J.: Permeability effects of deformation band arrays in sandstone, AAPG Bull., 88, 1315–1329, https://doi.org/10.1306/032804, 2004.

Stockmann, G. J., Wolff-Boenisch, D., Bovet, N., Gislason, S. R., and Oelkers, E. H.: The role of silicate surfaces on calcite precipitation kinetics, Geochim. Cosmochim. Act., 135, 231–250, https://doi.org/10.1016/j.gca.2014.03.015, 2014.

Taylor, W. L. and Pollard, D. D.: Estimation of in situ permeability of deformation bands in porous sandstone, Valley of Fire, Nevada, Water Resour. Res., 36, 2595–2606, https://doi.org/10.1029/2000WR900120, 2000.

Tenthorey, E., Scholz, C. H., Aharonov, E., and Leger, A.: Precipitation sealing and diagenesis 1. Experimental results, J. Geophys. Res.-Sol. Ea., 103, 23951–23967, https://doi.org/10.1029/98JB02229, 1998.

Torabi, A. and Fossen, H.: Spatial variation of microstructure and petrophysical properties along deformation bands in reservoir sandstones, AAPG Bull., 93, 919–938, https://doi.org/10.1306/03270908161, 2009.

Tueckmantel, C., Fisher, Q. J., Grattoni, C. A., and Aplin, A. C.: Single-and two-phase fluid flow properties of cataclastic fault rocks in porous sandstone, Mar. Pet. Geol., 29, 129–142, https://doi.org/10.1016/j.marpetgeo.2011.07.009, 2012.

Vai, G. B. and Martini, I. P. (Eds.): Anatomy of an orogen: The Apennines and Adjacent Mediterranean Basins, Dordrecht, Netherlands, Kluwer Academic Publishers, p. 637, 2001.

Walderhaug, O.: Modeling quartz cementation and porosity in middle Jurassic Brent Group sandstones of the Kvitebjørn field, Northern North Sea, AAPG Bull., 84, 1325–1339, 2000.

Whitworth, T. M., Haneberg, W. C., Mozley, P. S., and Goodwin, L. B.: Solute-sieving-induced calcite precipitation on pulverized quartz sand: experimental results and implications for the membrane behavior of fault gouge, in: Faults and Subsurface Fluid Flow in the Shallow Crust, edited by: Haneberg, W. C., Mozley, P. S., Moore, J. C., and Goodwin, L. B.,

American Geophysical Union, Washington, DC, 149–158, https://doi.org/10.1029/GM113p0149, 1999.

Wibberley, C. A. J., Petit, J.-P., and Rives, T.: The mechanics of fault distribution and localization in high-porosity sands, Provence, France, Geol. Soc. Spec. Publ., 289, 19–46, https://doi.org/10.1144/SP289.3, 2007.

Wilkins, S. J., Davies, R. K., and Naruk, S. J.: Subsurface observations of deformation bands and their impact on hydrocarbon production within the Holstein Field, Gulf of Mexico, USA, Geol. Soc. Spec. Publ., 496, 223–252, https://doi.org/10.1144/SP496-2018-139, 2019.

Williams, R. T., Farver, J. R., Onasch, C. M., and Winslow, D. F.: An experimental investigation of the role of microfracture surfaces in controlling quartz precipitation rate: applications to fault zone diagenesis, J. Struct. Geol., 74, 24–30, https://doi.org/10.1016/j.jsg.2015.02.011, 2015.

Williams, R. T., Goodwin, L. B., and Mozley, P. S.: Diagenetic controls on the evolution of fault-zone architecture and permeability structure: Implications for episodicity of fault-zone fluid transport in extensional basins, Geol. Soc. Am. Bull., 129, 464–478, https://doi.org/10.1130/B31443.1, 2016.

Wilson, J. E., Goodwin, L. B., and Lewis, C. J.: Deformation bands in nonwelded ignimbrites: Petrophysical controls on fault-zone deformation and evidence of preferential fluid flow, Geology, 31, 837–840, https://doi.org/10.1130/G19667R.1, 2003.

Wilson, J. E., Goodwin, L. B., and Lewis, C.: Diagenesis of deformation band faults: record and mechanical consequences of vadose zone flow and transport in the Bandelier Tuff, Los Alamos, New Mexico, J. Geophys. Res.-Sol. Ea., 111, B09201, https://doi.org/10.1029/2005JB003892, 2006.

Wollast, R.: Kinetic aspects of the nucleation and growth of calcite from aqueous solutions, in: Carbonate Cements, edited by: Bricker, O. P. and Mackenzie, F. T., J. Hopkins Press, 79, 264–273, 1971.